Review

Technology Landscape Review of Optical Microsystems and Photonics Integrated Circuits (PICs) for AI Sensing Applications

Hong Zhou *, Dongxiao Li, Chengkuo Lee *

Posted Date: 3 June 2025

doi: 10.20944/preprints202506.0169.v1

Keywords: Sensors; Photonic integrated circuits; artificial intelligence; surface-enhanced Raman spectroscopy; surface-enhanced infrared absorption; surface-enhanced fluorescence

 doi:10.20944/preprints202506.0169.v1

Review

Technology Landscape Review of Optical Microsystems and Photonics Integrated Circuits (PICs) for AI Sensing Applications

Hong Zhou [1,*], Dongxiao Li [2] and Chengkuo Lee [2,*]

[1] Ministry of Education Key Laboratory of Micro and Nano Systems for Aerospace, School of Mechanical Engineering, Northwestern Polytechnical University, Xi'an 710072, China
[2] Department of Electrical and Computer Engineering, National University of Singapore, Singapore 117583, Singapore
* Correspondence: zhouhong@nwpu.edu.cn (H.Z.); elelc@nus.edu.sg (C.L.)

Abstract: Optical sensors have undergone a significant evolution, transitioning from discrete optical microsystems toward sophisticated photonic integrated circuits (PICs) that leverage artificial intelligence (AI) for enhanced functionality. This review systematically explores the integration of optical sensing technologies with AI, charting the advancement from conventional optical microsystems to AI-driven smart devices. First, we examine classical optical sensing methodologies, including refractive index sensing, surface-enhanced infrared absorption (SEIRA), surface-enhanced Raman spectroscopy (SERS), surface plasmon-enhanced chiral spectroscopy, and surface-enhanced fluorescence (SEF) spectroscopy, highlighting their principles, capabilities, and limitations. Subsequently, we analyze the architecture of PIC-based sensing platforms, emphasizing their miniaturization, scalability, and real-time detection performance. The review then introduces the emerging paradigm of in-sensor computing, where AI algorithms are integrated directly within photonic devices, enabling real-time data processing, decision-making, and enhanced system autonomy. Finally, we offer a comprehensive outlook on current technological challenges and future research directions, addressing integration complexity, material compatibility, and data processing bottlenecks. This review provides timely insights into the transformative potential of AI-enhanced PIC sensors, setting the stage for future innovations in autonomous, intelligent sensing applications.

Keywords: sensors; photonic integrated circuits; artificial intelligence; surface-enhanced raman spectroscopy; surface-enhanced infrared absorption; surface-enhanced fluorescence

1. Introduction

Optical sensing technologies have undergone a dramatic evolution from early discrete microsystems to today's highly integrated smart photonic platforms [1]. Traditional optical sensors often required standalone components (lasers, lenses, detectors) assembled in bench-top or micro-optical setups, which limited their portability and scalability. The advent of photonic integrated circuits (PICs) has enabled the miniaturization of these optical systems onto millimeter-scale chips [2], drastically reducing size, weight, and alignment complexity. By amalgamating light sources, waveguides, modulators, and photodetectors on a single chip [3,4], PIC-based sensors can be more compact, energy-efficient, and cost-effective than their bulk optical predecessors. This integration is especially crucial for portable and wearable applications where size and power are at a premium [5].

At the same time, artificial intelligence (AI) has begun to play a transformative role in sensing [6–8]: machine learning algorithms are now routinely used to enhance signal processing, perform pattern recognition on complex optical spectra, and even control sensor operations in real-time. Marrying PIC technology with AI-driven data analysis has given rise to a new class of smart photonic sensors that can not only detect environmental or biochemical signals, but also interpret and respond

 doi:10.20944/preprints202506.0169.v1

to them autonomously [9]. For example, modern point-of-care diagnostic devices have combined nanophotonic sensor chips with AI-based spectral pattern recognition to identify pathogens within minutes [10] – a task that previously required lengthy laboratory analysis. Edge intelligence is emerging[11], whereby intensive computations are done locally at the sensor, enabling immediate decision-making without reliance on cloud computing. This trend toward on-chip intelligence is accelerating the development of photonic integrated circuit sensors that are AI-driven smart devices, capable of real-time sensing and interpretation.

In the following sections, we review the landscape of optical sensor technology leading up to this convergence (**Figure 1**). We first overview conventional optical sensing techniques – from refractive index (RI) sensing, surface-enhanced infrared absorption (SEIRA) spectroscopy, surface-enhanced Raman spectroscopy (SERS), surface plasmon-enhanced chiral spectroscopy to surface enhanced fluorescence (SEF) spectroscopy – which laid the groundwork for current systems. We then discuss representative applications of optical sensors in healthcare, environmental monitoring, and chemical detection. Next, we describe the architecture of photonic integrated circuits, and introduce the concept of in-sensor computing, where computational tasks are embedded within the sensor hardware. Finally, we examine current research frontiers and challenges, and provide an outlook on the future trajectory toward fully autonomous, miniaturized, and intelligent photonic sensing systems.

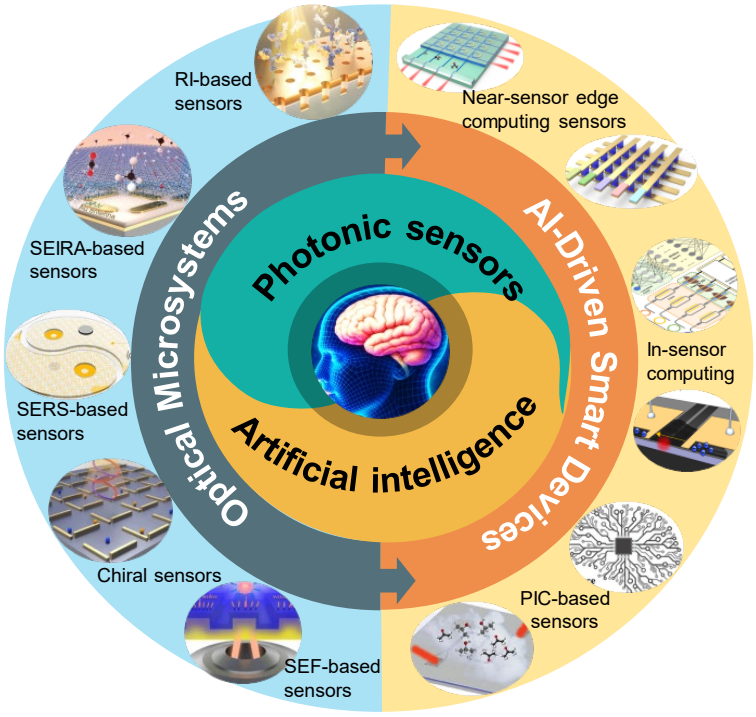

Figure 1. Optical sensing technologies toward AI-driven smart devices. RI: refractive index, SEIRA: surface-enhanced infrared absorption, SERS: surface-enhanced Raman spectroscopy, SEF: surface enhanced fluorescence.

2. Basic Sensing Technologies

Before the era of PICs, a rich variety of optical sensing methodologies were developed in free-space or fiber-optic formats [12–14]. These conventional optical sensors exploited different light–matter interaction mechanisms to detect physical, chemical, or biological quantities. Here we provide a brief overview of several important techniques: RI-based sensors, SEIRA-based sensors, SERS-based sensors, chiral sensors, and SEF-based sensors. Each of these approaches has distinct principles and strengths, and they continue to inform the design of integrated photonic sensors.

 doi:10.20944/preprints202506.0169.v1

2.1. RI Sensing

Surface plasmons offer an exceptionally sensitive route to refractive-index (RI) sensing by confining the electromagnetic field at the metal–dielectric interface [15–17]. Plasmon-based RI sensors combine several attractive features: high sensitivity (**Figure 2a**) [18,19], calibration-free operation, real-time monitoring, and non-invasive, label-free detection. By functionalizing the sensor surface with a thin film of biorecognition elements—for instance, antibodies, aptamers, or molecular imprints—one can selectively capture target analytes from biological, chemical, or gaseous samples. Upon binding, these targets alter the local RI near the plasmonic surface, which in turn shifts the resonance wavelength, amplitude, or phase of the plasmonic mode[20]. Tracking these signal variations provides kinetic information on molecular interactions, allowing quantitative analysis of specificity, binding affinity, and reaction dynamics. wo key figures of merit govern plasmonic RI sensor performance: the RI sensitivity (S_{RI}) and the sensor's figure of merit (FoM). Sensitivity is defined as [21]

$$S_{RI} = \frac{\Delta\lambda}{\Delta n} \quad (1)$$

where Δn is the change in refractive index and $\Delta\lambda$ is the corresponding shift in resonance wavelength. The FoM normalizes this sensitivity by the resonance linewidth, typically expressed as the full width at half maximum (FWHM), and is given by [22]

$$FoM = \frac{S_{RI}}{FWHM} \quad (2)$$

Higher values of S_{RI} and FoM both indicate superior sensor performance, reflecting greater wavelength shifts per RI unit and sharper resonance features for more precise detection.

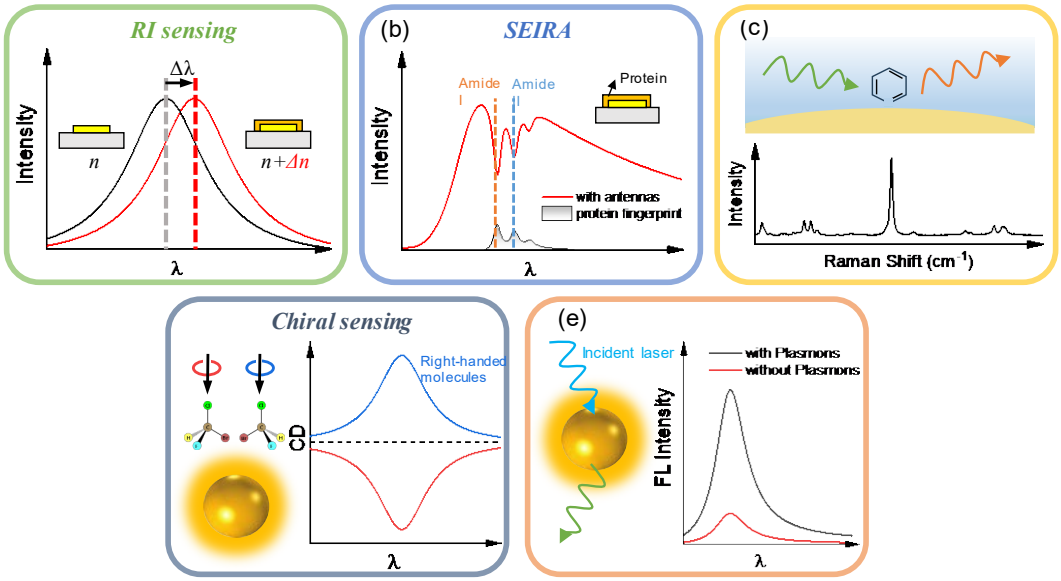

Figure 2. Mechanisms of photonic sensing. (a) RI-based sensing mechanism. (b) SEIRA-based sensing mechanism. (c) SERS-based sensing mechanism. (d) Chiral sensing mechanism. (e) SEF-based sensing mechanism.

2.2. Surface-Enhanced Infrared Absorption (SEIRA) Spectroscopy

Infrared spectroscopy offers a uniquely powerful window into biochemical systems by capturing the distinct vibrational "fingerprints" of their molecular constituents [23–25]. Its intrinsic chemical specificity, coupled with label-free, non-invasive, real-time measurement capabilities, has driven breakthroughs in fields ranging from environmental surveillance and defense to chemical analysis and medical diagnostics. Yet traditional infrared methods suffer from inherently low sensitivity when probing molecules whose absorption cross-sections are tiny compared to the micron-scale wavelengths of IR light [26–28].

 doi:10.20944/preprints202506.0169.v1

Plasmonic nanoantennas remedy this mismatch by funneling and concentrating incident radiation into nanoscale "hot spots," where the local electromagnetic field is dramatically intensified. This strong light–matter coupling enables detection of otherwise weak vibrational features—a phenomenon known as surface-enhanced infrared absorption (SEIRA) spectroscopy (**Figure 2b**) [6]. The standard figure of merit for SEIRA performance is the enhancement factor (EF), defined as

$$EF = \frac{I_{SEIRA}}{I_{ref}} \frac{N_{ref}}{N_{SEIRA}} \quad (3)$$

where I_{SEIRA} is the vibrational absorption intensity after plasmonic coupling, I_{ref} is the corresponding intensity for an uncoupled (pure) molecular sample, N_{SEIRA} denotes the number of molecules located within the antenna's electromagnetic hot spots, and N_{ref} is the total number of molecules in the reference measurement. This metric thus captures both the optical "gain" provided by the antenna and the fraction of molecules experiencing that enhancement.

2.3. Surface-Enhanced Raman Spectroscopy (SERS)

Raman spectroscopy probes the vibrational and rotational modes of molecules and crystal lattices through inelastic scattering [29–31]. When a sample is illuminated with a laser or other monochromatic light, its molecules vibrate and scatter photons at shifted frequencies. By measuring the frequency shifts and intensities of this scattered light, Raman spectroscopy reveals detailed information about molecular structure and bonding. However, because spontaneous Raman scattering is inherently weak and often overwhelmed by much stronger Rayleigh (elastic) scattering, its sensitivity is limited.

Surface-enhanced Raman scattering (SERS) overcomes this drawback by amplifying the Raman signal by several orders of magnitude (**Figure 2c**) [32–34]. In SERS, metal nanostructures—typically silver or gold nanoparticles—serve as "hot spots" that concentrate and enhance the local electromagnetic field (electromagnetic enhancement) and facilitate charge transfer between the substrate and adsorbed molecules (chemical enhancement). A SERS substrate is created by depositing these nanoparticles onto a surface, dramatically boosting the intensity of the scattered light. The calculation formula of SERS intensity is,

$$I_{SERS} \cong I_0 \left| \frac{E(\omega_{ext}) E(\omega_{det})}{E_0(\omega_{ext}) E_0(\omega_{det})} \right|^2 \quad (4)$$

Among them, the enhancement factor (EF) scales with the square of the ratio between the enhanced local field strength (E) and the incident field strength (E_0), evaluated at both the excitation frequency (ω_{ext}) and the Raman detection frequency (ω_{det}). Thanks to its ultra-high sensitivity and molecular selectivity, SERS has rapidly become a powerful tool for detecting trace analytes. Advances in SERS theory, substrate engineering, and instrumentation have expanded its applications across biomedical diagnostics, nanomaterial characterization, food safety testing, and environmental monitoring.

2.4. Surface Plasmon-Enhanced Chiral Spectroscopy

Chiral molecules are those whose structures cannot be superimposed on their mirror images by any combination of rotations or translations (**Figure 2d**) [35–37]. As a result, each chiral compound exists as two distinct, non-overlapping forms called enantiomers. Chirality is a fundamental characteristic found throughout nature, particularly in biomolecules: for instance, amino acids and nucleic acids each occur as left- and right-handed versions. Although both enantiomers share identical elemental composition and functional groups, their chemical behaviors can differ dramatically. This distinction is especially critical in pharmaceuticals and agrochemicals, where one enantiomer may be therapeutically active while its counterpart is inert or even harmful. Consequently, the ability to detect and differentiate between enantiomers is essential across analytical chemistry, biomedicine, drug manufacturing, and toxicology. Traditional techniques such as optical rotatory dispersion (ORD) and circular dichroism (CD) spectroscopy are routinely employed to probe

 doi:10.20944/preprints202506.0169.v1

molecular chirality. However, because the helical pitch of many chiral molecules is much smaller than the wavelength of visible light, these conventional methods often struggle to capture chiral signals from minute sample volumes. Recent breakthroughs in nanophotonics offer promising solutions: for example, engineered metasurfaces with chiral architectures can generate areas of intense optical chirality and boost CD responses, thereby amplifying otherwise weak chiral signatures.

2.5. Surface-Enhanced Fluorescence (SEF) Spectroscopy

Fluorescence detection is a cornerstone of life-science research and medical diagnostics because it offers exceptionally low detection limits and a wide variety of fluorophores, enabling the simultaneous monitoring of multiple biomarkers [38–40]. However, at low analyte concentrations, the emitted fluorescence can become exceedingly weak, necessitating sophisticated, costly, and often bulky equipment to preserve high sensitivity. Such large instruments are impractical for disease diagnosis in resource-constrained environments. In recent years, plasmonic nanostructures composed of noble metals have emerged as an elegant strategy to amplify fluorophore signals without complex hardware. When illuminated, metal nanoparticles support localized surface-plasmon resonances at their metal–dielectric boundaries, intensifying the nearby electromagnetic field and boosting the fluorophore's excitation rate. Simultaneously, an elevated local density of optical states enhances the fluorophore's emission probability, shortening its fluorescence lifetime and raising its quantum yield. By positioning fluorophores in close proximity to conductive metal surfaces or particles, one harnesses this surface-enhanced fluorescence (SEF) phenomenon (**Figure 2e**) to achieve much stronger signals with simpler, more compact platforms.

3. Applications of Optical Sensors

3.1. Refractive Index Sensing

Plasmonic refractive-index sensors have become invaluable tools in biological research and clinical diagnostics owing to their simplicity and affordability. Unlike conventional methods such as enzyme-linked immunosorbent assays (ELISA) or polymerase chain reaction (PCR), plasmonic RI sensors enable noninvasive, real-time, label-free, and rapid biomarker quantification. A prominent example is the detection of prostate-specific antigen (PSA), a key indicator used in prostate cancer screening[41]. In healthy individuals, PSA levels typically range from 4.0 to 10 ng/mL[42], while concentrations exceeding 10 ng/mL signal an elevated cancer risk. Early and accurate PSA measurement is therefore critical. In 2018, Khan et al. designed a gold nanodisc array functionalized with PSA-specific DNA aptamers (**Figure 3a**)[43]. By tuning the nanodisc dimensions, they achieved a localized plasmon resonance at 646 nm. This aptamer-modified platform delivered a sensitivity of 113 nm/RIU, a detection limit as low as 1.49 ng/mL, and a dynamic range spanning 1.7–20.4 ng/mL.

Beyond protein markers, plasmonic RI sensors can also target tumor-derived exosomes—50–150 nm extracellular vesicles present in bodily fluids such as blood, urine, and saliva[44–48]—that mediate intercellular communication by ferrying molecular cargo[49–51]. Elevated exosome levels have been correlated with malignancy, making them promising diagnostic biomarkers. However, traditional exosome assays often demand extensive sample purification and labeling, hindering device miniaturization and point-of-care deployment[52]. To overcome these challenges, Lm et al. introduced the nanoplasmonic exosome (nPLEX) assay[53], which employs periodic nanohole arrays to induce strong surface plasmon resonances. Exosome binding shifts the resonance signal, and quantitative analysis is performed by monitoring phase or intensity changes; matching the array periodicity to exosome size further enhances sensitivity. Building on this, Lim and colleagues later developed the amplified plasmonic exosome (APEX) platform (**Figure 3b**)[54], which uses localized optical deposition and in situ enzymatic transformation on bilayer plasmonic nanostructures for multiplexed exosome profiling. This approach achieves a sensitivity of approximately 200 exosomes and can distinguish between exosome-bound and unbound amyloid β populations directly in blood, offering a minimally invasive means to assess cerebral plaque burden in Alzheimer's disease.

 doi:10.20944/preprints202506.0169.v1

The COVID-19 pandemic has underscored the urgent need for rapid, reliable diagnostics[55], particularly in resource-limited settings where shortages of medical infrastructure can hinder containment efforts and increase morbidity and mortality among vulnerable populations[56,57]. Although numerous antigen- and antibody-based assays have been developed for SARS-CoV-2 detection[58,59], plasmonic RI sensors stand out for their label-free, real-time operation[60–63]. For instance, Funari and colleagues engineered a gold-nanospike optofluidic platform that exploits localized surface plasmon resonance (LSPR) to detect anti-spike protein antibodies in plasmon[64]. Antigen–antibody binding alters the local refractive index around the nanospikes, producing a measurable red shift in the LSPR peak; this system achieves a sensitivity of 183 nm/RIU and a detection limit of 0.5 pM[65–67]. Similar plasmonic RI approaches have since been applied to the detection of other viral targets, demonstrating the broad applicability of this technology.

Despite their sensitivity, conventional plasmonic setups often rely on high-performance spectrometers that are bulky, costly, and complex—obstacles to widespread adoption in point-of-care and field settings. To address these limitations[68,69], researchers have developed spatial-multiplexing metasurfaces that encode refractive-index changes as variations in far-field intensity patterns. By illuminating a gradient or pixelated metasurface with narrowband light and capturing its position-dependent scattering with a simple camera[70], one can monitor analyte binding events through real-time intensity shifts, obviating the need for precision spectrometers[71–73]. This strategy has yielded remarkably sensitive and streamlined sensing platforms. For example, Ansaryan et al. introduced a label-free nanoplasmonic imaging system that maps single-cell secretions in a microwell array (**Figure 3c**)[74]: gold nanohole arrays support the plasmon resonances, and a complementary-metal-oxide camera records intensity changes driven by molecular attachment. Coupled with machine-learning–based image analysis, this approach enables high-throughput, spatiotemporal monitoring of hundreds of individual cells, paving the way for parallelized, real-time molecular diagnostics.

Optical fibers have emerged as a powerful platform for biosensing in early medical diagnostics due to their low cost, mechanical flexibility, compact form factor, immunity to electromagnetic interference, and suitability for remote monitoring. However, their inherently modest sensitivity has posed a major challenge for detecting low-abundance biomarkers. To address this, researchers have harnessed localized surface plasmon resonance (LSPR) in metallic nanostructures to amplify the evanescent field at the fiber surface, markedly boosting sensor performance.

Building on these advances, plasmonic optical microfiber biosensors have been shown to detect individual biomolecules and nanoparticles ranging from roughly 50 to 500 nm in diameter[75–79]. In a notable extension of this concept, Huang and colleagues engineered a dual-amplification interface that couples plasmonic enhancement with an aptamer-driven conformational switch (**Figure 3d**). This design enables single-molecule sensing of small targets such as dopamine in complex biological fluids[80]—achieving detection limits down to approximately 1.3 attomolar in cerebrospinal fluid, 1.5 attomolar in whole serum, and 0.5 attomolar in artificial sweat. By simply exchanging the aptamer sequence, the same platform can be adapted to sense a wide variety of other small molecules and ions at the single-molecule level[81–84].

 doi:10.20944/preprints202506.0169.v1

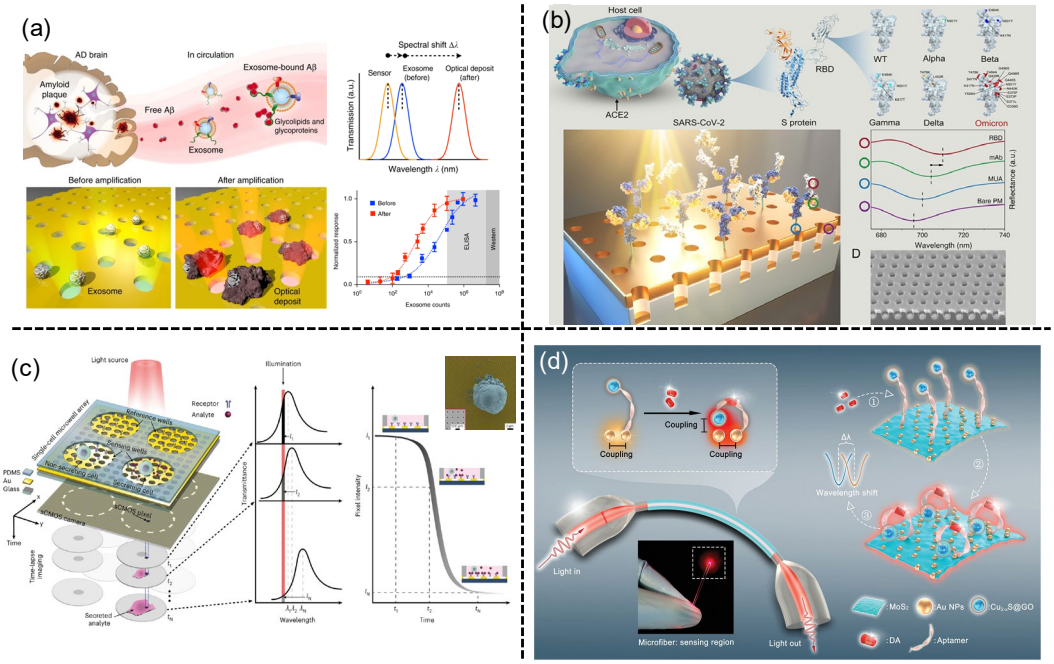

Figure 3. RI-based sensing applications. (a) RI-based sensors for subtyping of circulating exosome-bound amyloid β reflects brain plaque deposition[43]. (b) RI-based sensors for label-free immunoassay boosting[54]. (c) RI-based sensors for high-throughput spatiotemporal monitoring of single-cell secretions[74]. (d) RI-based sensors for single-molecule and noninvasive dopamine detection[80].

3.2. Surface-Enhanced Infrared Absorption Spectroscopy

Although refractive index (RI) sensors offer user-friendly operation and high sensitivity, they are inherently limited by the fact that shifts in resonant frequency alone cannot reveal molecular identity, constraining their ability to distinguish between different analytes. Infrared absorption spectroscopy addresses this shortcoming by providing chemical-specific information via characteristic spectral fingerprints. Yet, the inherently low absorption cross-section of most molecules renders conventional infrared techniques insufficiently sensitive for detecting trace concentrations[85,86]. Surface-enhanced infrared absorption (SEIRA) spectroscopy overcomes this barrier by exploiting plasmonic enhancement to amplify weak molecular signals[87–89]. First observed by Hartstein and colleagues in 1980 using randomly distributed metal island films[90], early SEIRA platforms suffered from non-resonant enhancement and modest field amplification (typically on the order of 10^1–10^2)[91,92]. The advent of engineered metasurfaces—with their precisely defined, periodic geometries—has revolutionized SEIRA[93–97], enabling higher and tunable resonance enhancement. Advances in micro- and nanofabrication have yielded a rich variety of metasurface motifs, including asymmetric crosses[98,99], split-ring resonators[100], and fractal architectures[101,102], each offering tailored control over electromagnetic fields to boost SEIRA performance. Nonetheless, these designs often remain constrained by human intuition, favoring simple two-dimensional geometries over potentially richer, multidimensional configurations[103].

Maximizing the spatial overlap between target molecules and the intense near-field “hot spots” around nanoantennas is equally crucial for SEIRA sensitivity. A significant portion of the enhanced field typically resides within the underlying dielectric substrate, limiting direct interaction with analyte molecules. To address this, researchers have developed nanopedestal platforms by etching away portions of the dielectric[104–106], thereby elevating the plasmonic elements into free space and increasing the overlap between molecules and hot spots. Compared to planar nanoantennas, these nanopedestals can deliver a 2.5–10-fold improvement in SEIRA sensitivity[105], further augmented by their passive ability to capture and concentrate analytes[107]. Alternatively, coating nanoantenna surfaces with molecule-enriching layers or functionalizing them with specific probe ligands has proven effective for selective adsorption of proteins, nucleic acids, and lipids in liquid

 doi:10.20944/preprints202506.0169.v1

environments. Such chemical tailoring enables dynamic, real-time SEIRA detection of low-abundance biomolecules, broadening the technique's applicability in biosensing and diagnostics (**Figure 4a**)[85,108–113].

Machine learning has accelerated advances in SEIRA spectroscopy (**Figure 4b**) [114–116]. For instance, Kavungal et al. combined an immunoassay with a nanoplasmonic infrared metasurface to selectively detect proteins implicated in neurodegenerative disorders[117]. By training an artificial neural network on the sensor's spectral response, they achieved highly accurate quantification of complex mixtures containing both oligomeric and fibrillar aggregates. While SEIRA offers powerful insights into molecular dynamics, conventional infrared spectroscopy often struggles to disentangle overlapping vibrational bands. To address this, Zhou et al. engineered vertically stacked infrared nanoantennas that harness the hybridization between localized surface plasmons and surface phonon polaritons (SPhPs) [118]. Operating within the Reststrahlen band, these SPhPs exhibit extreme refractive-index sensitivity; when paired with deep-learning algorithms, this platform can deconvolve strongly overlapping vibrational signatures arising during biological reactions.

In parallel, several strategies have emerged to push SEIRA sensitivity even further. Optimization of plasmonic loss profiles[119–121] and the synthesis of complex-frequency excitation waveforms[122] have both demonstrated appreciable gains in signal strength. Meanwhile, molecular-enrichment coatings have proven highly effective for trace-gas detection[123–127]. For example, Zhou et al. applied a ZIF-8 film to capture and concentrate gas molecules on the sensor surface, yielding a significant boost in sensitivity (Figure 4c) [128]. Building on this approach, they subsequently employed MOF/polymer hybrid films to drive the CO_2 detection limit down into the sub-parts-per-million regime[129].

Enhancing spectral bandwidth is another key objective in SEIRA, since broadband measurements capture richer molecular fingerprints for more precise identification and retrieval. To this end, a variety of metasurface architectures have been proposed to realize broadband or multiband plasmonic resonances, including fractal geometries[101,102,130], self-similar scaffolds[131,132], asymmetric resonators[98], gradient metasurfaces[133,134], and supercell designs[116]. A common approach is to co-locate nanoantennas tuned to different frequencies within a single unit cell[135]; however, as antenna density increases, so does inter-antenna coupling. Supercells—arrays of 16 hook-shaped nanoantenna sub-cells with gradually varying dimensions—effectively suppress this coupling and yield a continuous resonance spanning 6–9 μm (**Figure 4d**) [116]. Alternatively, stitching discrete resonances into a contiguous spectrum via spatial multiplexing establishes a one-to-one mapping between wavelength and position, enabling spectrometer-free detection[136–139], though at the expense of larger device footprints. To overcome this trade-off, Li et al. applied coupled-mode theory to design an overcoupled metamaterial absorber that delivers uniform enhancement across 6–14 μm, allowing fingerprint retrieval of 13 analytes with a single metasurface array for the first time (**Figure 4e**) [115]. The broadband performance of such overcoupled resonators has since been further validated by Paggi et al. [140]

 doi:10.20944/preprints202506.0169.v1

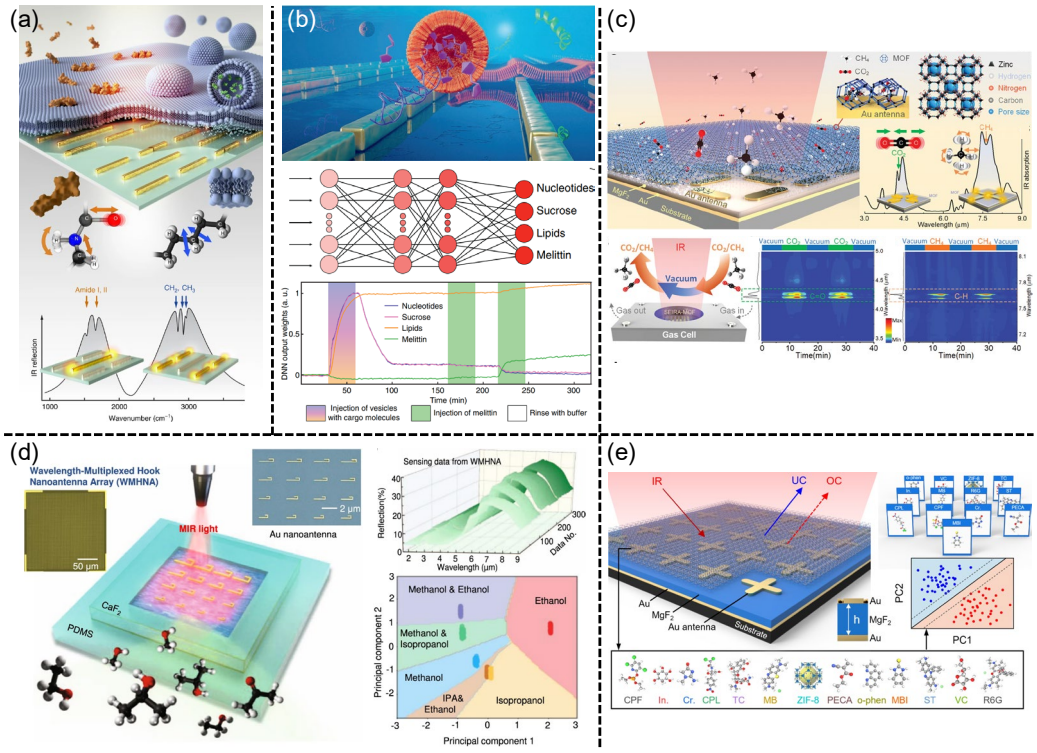

Figure 4. SEIRA-based sensing applications. (a) Multi-resonant SEIRA-based sensors for the detection of lipid membrane[104]. (b) SEIRA-based sensors for monitoring dynamics between all major classes of biomolecules[125]. (c) SEIRA-based sensors for simultaneous on-chip sensing of greenhouse gases[128]. (d) SEIRA-based sensors using wavelength-multiplexed hook nanoantennas[116]. (e) Ultrasensitive molecular fingerprint retrieval using strongly detuned overcoupled plasmonic nanoantennas[115].

3.3. Surface-Enhanced Raman Spectroscopy

Raman spectroscopy serves as an invaluable complement to infrared absorption techniques. Although both probe molecular vibrations, infrared spectroscopy measures absorption while Raman relies on inelastic light scattering. Moreover, the strong absorption of mid-infrared light by water severely limits IR-based measurements in aqueous environments, whereas water's inelastic Raman scattering cross section is negligible. Consequently, Raman methods can capture vibrational fingerprints in high-water-content contexts—such as biological fluids or intracellular milieus—where infrared fails. Yet, the inherently weak Raman cross sections of most molecules impede detection at low concentrations. SERS overcomes this limitation by exploiting plasmon-mediated electric-field amplification (and, in some cases, chemical enhancement) to boost Raman signals of trace analytes. First observed serendipitously by Fleischmann and colleagues—who noted dramatically increased Raman intensity of pyridine on roughened silver electrodes—SERS has since evolved into a robust technique celebrated for its ultra-high sensitivity and molecular specificity, with applications spanning surface/interface chemistry, life sciences, clinical diagnostics, food safety, and environmental monitoring.

Surfaces and interfaces underpin critical phenomena in heterogeneous catalysis, electrochemistry, and photo(electro)chemistry, yet elucidating their molecular-scale behavior demands techniques with exceptional surface sensitivity. SERS excels in this regard. For example, Yu et al. introduced a depth-sensitive, plasma-enhanced Raman approach to probe both the nanostructure and chemical composition of the solid-electrolyte interphase (SEI) on lithium metal anodes (**Figure 5a**) [141]. Their dynamic, molecular-level insights into SEI formation and evolution offer a powerful guide for engineering more stable and higher-performance battery interfaces. Beyond energy storage, the combination of high spatial resolution and sub-nanometer hot spots in SERS substrates enables nanoscale chemical mapping and even single-molecule optomechanical studies.

 doi:10.20944/preprints202506.0169.v1

The rich vibrational fingerprints accessible via SERS also pave the way for "photonic noses" and "photonic tongues." Inspired by biological olfaction, Kim et al. fabricated an array of eight SERS substrates, each functionalized with a unique self-assembled monolayer, to create a receptor-agnostic sensing platform. By capturing multifaceted spectral signatures, this artificial-nose design achieves high-accuracy discrimination of complex biological samples without relying on target-specific receptors. Similarly, Leong et al. developed a breathalyzer based on SERS for non-invasive COVID-19 screening, demonstrating 96.2% sensitivity and 99.9% specificity (**Figure 5b**) [142]. Extending SERS into liquid sensing, Ling and colleagues engineered a "SERS taster" for multiplexed analysis of wine aromas (**Figure 5c**) [143]. By integrating multiple non-covalent receptor chemistries and constructing comprehensive "SERS superprofiles," they achieved predictive flavor analytics via chemometric modeling. Together, these advances underscore SERS's versatility in delivering molecular-level insights across both dry and liquid environments, and they highlight its central role in next-generation photonic sensing platforms.

The inherent rigidity of conventional SERS substrates poses a fundamental challenge for wearable applications on soft, dynamic biological surfaces. To bridge this mechanical mismatch, recent efforts have focused on engineering flexible, skin-conformable SERS platforms. For example, Wang et al. developed a stretchable plasmonic metasurface sensor that seamlessly integrates a flexible SERS-active metasurface with a compliant microfluidic system for continuous sweat sampling (**Figure 5d**) [144]. By harvesting analytes directly from epidermal sweat and exploiting each molecule's unique Raman fingerprint, this device enables non-invasive, real-time molecular profiling. Building on this concept, Mogera et al. introduced a plasmonic-paper–based microfluidic wearable that concurrently quantifies sweat volume, rate, and metabolite concentrations (**Figure 5e**) [145]. Their integrated sensor achieves sensitive detection of uric acid down to 1 μM in perspiration, demonstrating the promise of flexible SERS wearables for personalized health monitoring, point-of-care diagnostics, and responsive drug delivery systems.

Beyond human health, SERS has found emerging application in plant physiology and agricultural management. Plants under biotic or abiotic stress secrete signaling metabolites—such as salicylic acid, extracellular ATP, phytoalexins, and glutathione—that govern defense pathways. Traditional assays often require destructive sampling, hindering real-time assessment. Addressing this, Son et al. introduced SERS nanoprobes into the plant apoplast to non-invasively track endogenous signaling molecules in situ (**Figure 5f**) [146]. Their approach successfully detected key stress markers in living nasturtium, wheat, and barley, providing dynamic insights into plant responses. Moreover, SERS platforms have been leveraged to monitor pesticide residues, illicit additives, and mycotoxins on harvested produce. Collectively, these advances highlight SERS's versatility as a high-sensitivity, surface-specific tool for precision agriculture, where rapid, on-site analysis can optimize crop health, resource utilization, and yield quality.

 doi:10.20944/preprints202506.0169.v1

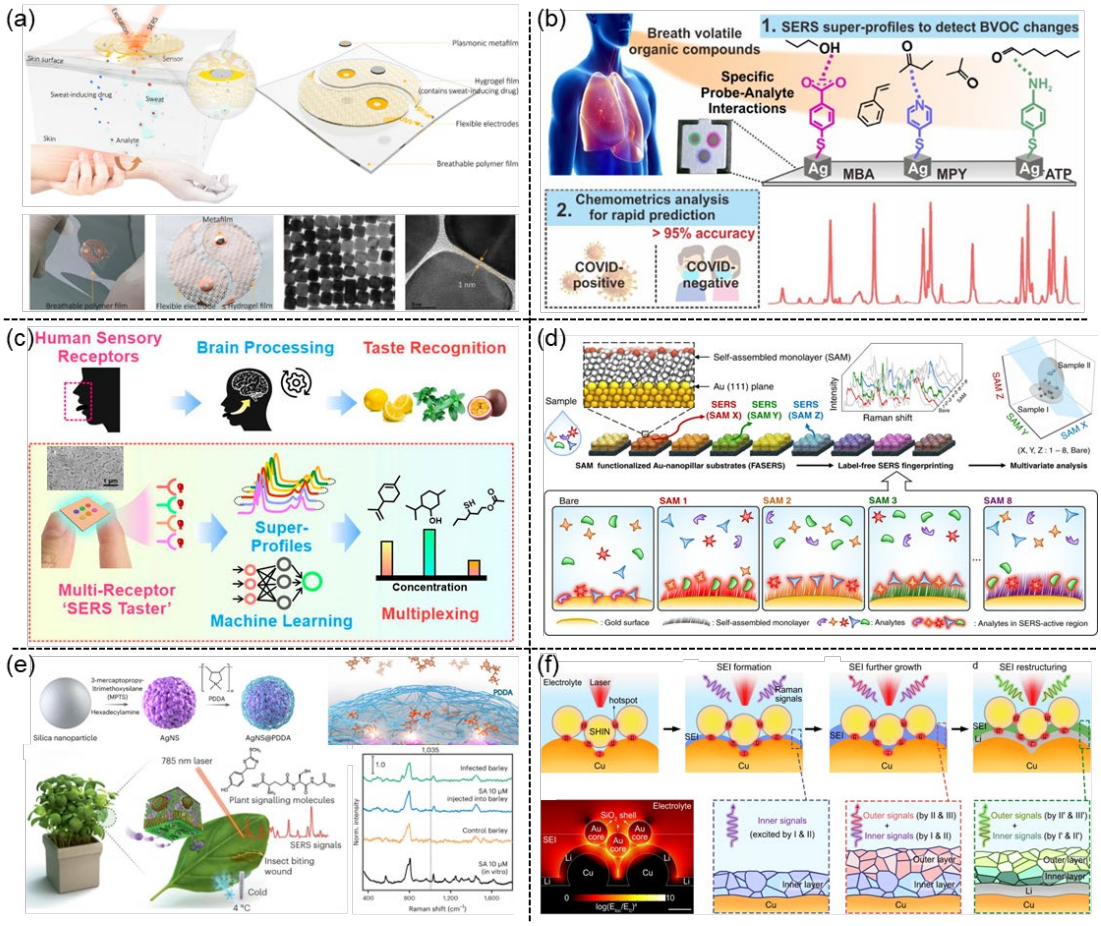

Figure 5. SERS-based sensing applications. (a) SERS-based nanosensor for resolving nanostructure and chemistry of solid-electrolyte interphase on lithium anodes[141]. (b) Noninvasive and point-of-care SERS-based breathalyzer[142]. (c) SERS-based nanosensor for multiplex profiling of wine flavors[143]. (d) Wearable plasmonic-metasurface sensor[144]. (e) SERS-based nose for high dimensionality fingerprinting[145]. (f) SERS-based nanosensor for the real-time monitoring of multiple stress signalling molecules in plants[146].

3.4. Surface Plasmon-Enhanced Chiral Spectroscopy

Differentiating enantiomeric species is vital across biomedical, pharmaceutical, and chemical analyses, yet traditional circular dichroism (CD) spectroscopy suffers from intrinsically weak signals—often on the order of 10^{-5}. To overcome this, chiral plasmonic architectures have been developed to amplify CD responses. In 2018, Zhao et al. introduced planar plasmonic metamaterials with enantiomorphic patterns that significantly enhance CD detection of diverse proteins (**Figure 6a**) [147]. Building on this concept, Kadodwala and co-workers fabricated arrays of metallic "gamma" motifs in left- or right-handed orientations[148]. These arrays convert incident linearly polarized light into elliptically polarized modes of fixed handedness; when chiral biomolecules adsorb, the refractive-index–sensitive plasmon resonance shifts differently under left- versus right-circularly polarized excitation, yielding a differential signal. Such plasmonic enhancement can boost chiral sensitivity by up to six orders of magnitude compared to conventional CD. Later, the same group designed shuriken-shaped metasurfaces that further improve chiral asymmetry and spatial confinement, enabling sensitive detection of viruses[149], antibodies[150], and peptide assemblies[151]. All-dielectric nanostructures have also been employed to generate strong, uniform chiral near fields (**Figure 6b–c**) [152,153], offering an alternative route to plasmonic approaches.

While most CD measurements reside in the ultraviolet–visible–near-infrared range—where molecular electronic transitions give stronger signals—these wavelengths often lack the detailed structural insight needed to distinguish complex chiral mixtures. Extending CD into the mid-infrared to access vibrational circular dichroism (VCD) addresses this gap by probing chiral vibrational

 doi:10.20944/preprints202506.0169.v1

transitions[154]. However, VCD signals are inherently 10^2–10^3 times weaker than electronic CD, limiting sensitivity. Plasmonic platforms offer a solution: Chanda's team demonstrated a four-order–of–magnitude enhancement of VCD using an achiral plasmonic substrate[155], and subsequent tuning of the same system achieved up to 10^{13}-fold sensitivity gains. To elucidate the mechanism behind this dramatic amplification, Xu et al. explored the relationship between near-field coupling and far-field CD. By selectively masking nanogaps in a four-resonator metamaterial and systematically varying coupling strength, they confirmed that intensified chiral near fields drive the far-field CD response[156]. Capitalizing on these insights, Xu and colleagues then developed a plasmonic chiral metamaterial platform for surface-enhanced VCD, demonstrating the first label-free discrimination of protein secondary structures and the direct analysis of chiral mixtures via enhanced VCD spectroscopy (**Figure 6d**) [157]. This work charts a path toward ultra-low–volume, high–sensitivity chiral detection with molecular structural resolution.

Raman optical activity (ROA) has recently gained traction as a complementary chiral-spectroscopy modality, particularly for aqueous samples that strongly absorb in the mid-IR and thus challenge VCD[158]. Like ROA, however, its inherently weak signal necessitates enhancement strategies. Early theoretical groundwork by Efrima in 1983 first established the feasibility of surface-enhanced ROA and introduced the foundational treatment of substrate-induced modifications to molecular response tensors. Building on this, Janesko et al. formulated an electromagnetic-enhancement model that elegantly marries the standard ROA formalism with plasmon-mediated field amplification[159]. Experimentally, Sun and colleagues exploited silver chiral nanowires as plasmonic waveguides to boost ROA intensities, enabling clear discrimination of Raman responses under left- versus right-circularly polarized excitation and thus precise determination of molecular chirality and conformation[160]. More recently, Ostovar's team identified a chiral-transfer mechanism whereby achiral nanoparticles, upon interaction with adjacent chiral species, undergo symmetry breaking in their excitation fields; this asymmetry between LCP and RCP absorption manifests as a detectable ROA signal even from nominally achiral substrates[161].

Extending circular-dichroism techniques into the terahertz (THz) regime promises access to both vibrational and rotational signatures of biomacromolecules, but the lack of efficient THz polarization modulators has long stymied terahertz circular dichroism (TCD) spectroscopy[162]. Innovations in nonlinear metasurfaces are now overcoming this barrier: Choi et al. employed kirigami-patterned plasmonic sheets whose tunable mechanical deformation yields over 80° of polarization rotation across thousands of actuation cycles, enabling dynamic modulation of THz circular polarization[163]. In parallel, McDonnell and colleagues developed a broadband THz emitter based on Pancharatnam–Berry–phase nonlinear metasurfaces, which affords simultaneous control of the emitted wave's phase and handedness[164]. Leveraging these modulators, they demonstrated bona fide TCD measurements, unlocking the capability to detect chiral phonon modes in biomolecular crystals[165] and opening vistas for THz-enabled studies of biochemical dynamics and medical diagnostics[166]. Looking ahead, tunable chiral metasurfaces assembled via colloidal self-organization (**Figure 6f**) [167] offer additional degrees of freedom, heralding a new generation of reconfigurable TCD platforms.

 doi:10.20944/preprints202506.0169.v1

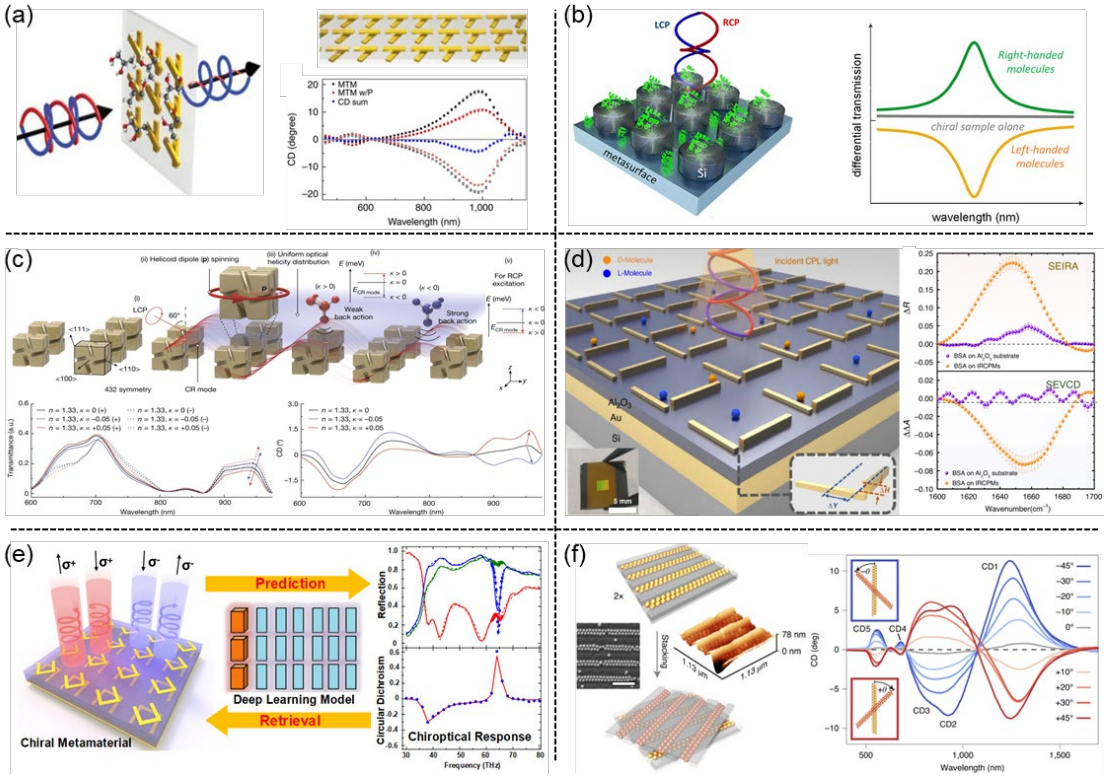

Figure 6. Chiral sensing applications. (a) Chirality detection of enantiomers using twisted optical metamaterials[147]. (b) Accessible Superchiral Near-Fields Driven by Tailored Electric and Magnetic Resonances in All-Dielectric Nanostructures[152]. (c) Enantioselective sensing by collective circular dichroism[153]. (d) Expanding chiral metamaterials for retrieving fingerprints via vibrational circular dichroism[157]. (e) On-demand design of chiral metamaterials[162]. (f) Mechano-tunable chiral metasurfaces via colloidal assembly[167].

3.5. Surface Enhanced Fluorescence Spectroscopy

Surface-enhanced fluorescence (SEF) harnesses plasmonic near-fields to dramatically amplify molecular emission, enabling detection and imaging down to the single-molecule level. The phenomenon was first observed in the 1960s by Drexhage et al., who correlated fluorophore decay rates with its distance from a metallic film[168]. Building on this, Lakowicz, Geddes, and coworkers conducted extensive studies throughout the 1980s and ’90s, demonstrating that roughened silver island films could both enhance fluorescence intensity and modify lifetimes[169–174]. With advances in colloidal synthesis, well-defined noble metal nanoparticles—spheres, rods, shells, and bowties—have supplanted island films as SEF substrates[175–181]. In a landmark experiment, Kühn et al. used a scanning-probe tip to position a single dye molecule adjacent to a solitary gold nanoparticle, achieving over 20× fluorescence enhancement[182]. Recognizing the need for directional plasmon modes, later designs employed nanoshells, nanorods, nanopores, and bowtie antennas to concentrate fields in sub-10 nm gaps, yielding substantially higher enhancements[183–188]. For example, Xiong and colleagues exploited photonic-crystal cavities to boost quantum-dot emission and suppress blinking—key improvements for biosensing platforms (**Figure 7a**) [40]. Kinkhabwala’s team further pushed enhancement limits by fabricating 14 nm-gap gold bowties via electron-beam lithography, reporting up to 1,340× fluorescence gains for dyes located in the nanogap.

Single-molecule sensitivity remains a signature application of SEF. In 2007, Lakowicz et al. detected individual rhodamine molecules on silver island substrates, observing a 7× intensity increase and reduced lifetime[189]. Orrit’s group subsequently demonstrated wet-chemical synthesis of gold nanorods that rival lithographic components, achieving >1,000× enhancement of crystal violet fluorescence with a 2% quantum yield[188]. More recent innovations include plasmonic “add-on” labels that integrate seamlessly with existing bioassays to boost signal-to-noise and dynamic range

 doi:10.20944/preprints202506.0169.v1

without altering protocols (**Figure 7b**) [190]. Lin et al. introduced a multiplexed enhanced-fluorescence microarray immunoassay (eFMIA) built on nanostructured gold nanoislands, which macroscopically amplified near-infrared emission of IRDye78 by 202.6× (**Figure 7c**) [191]. Together, these advances underscore SEF's transformative potential for ultra-sensitive fluorescence diagnostics and high-throughput biosensing.

Detection of amino acids and proteins via SEF holds great promise for early disease risk assessment, given the fundamental role of amino acids as protein building blocks. Lakowicz and co-workers pioneered the use of aluminum-nanoparticle substrates for label-free amino-acid sensing, achieving up to a 3,500-fold enhancement when fluorophores align perpendicularly to the metal surface[192]. They further demonstrated significant fluorescence boosts for intrinsic tryptophan and tyrosine emissions on aluminum nanoparticles. Geddes's group extended SEF to protein detection, initially profiling erythrin and algal proteins on roughened metallic films and later recombinant targets. More recently, aptamer-based sensors have emerged as a versatile platform: Chen et al. engineered a bivalent DNA-aptamer labeled with FITC and anchored to silver nanoparticles, minimizing dye–nanoparticle separation and yielding a sensitivity three orders of magnitude greater than conventional homogeneous assays, with an LOD of 1.25 pM[193]. These advances underscore SEF's potential for ultra-sensitive biomarker assays and early diagnostic applications.

Beyond static detection, SEF is increasingly applied to monitor single-molecule reaction dynamics. Li and colleagues utilized a plasmonic nanocavity to co-enhance fluorescence and Raman signatures of individual rhodamine B isothiocyanate molecules (**Figure 7d**) [194]. By tracking shifts in the fluorescence emission band due to conformational changes and simultaneously identifying transient reaction intermediates via their Raman fingerprints, they achieved real-time, single-molecule resolution of photochemical cleavage mechanisms. This correlative spectroscopy approach provides unprecedented insight into reaction pathways at the molecular level[195–197].

SEF's utility extends to microbiological detection, a critical need in public-health surveillance. Lakhtakia's team first reported SEF-based E. coli detection on porous metal-engraved films (Ag, Al, Au, Cu), achieving ~20× fluorescence enhancement over glass substrates[198]. Knoll et al. improved upon this by employing mixed-thiol SAMs on gold to support long-range surface plasmons, detecting E. coli down to <10 CFU/mL across a 10–10^6 CFU/mL range. The COVID-19 pandemic has further accelerated SEF viral diagnostics: Hu et al. developed nanostructured gold chips for multiplexed antibody profiling against SARS-CoV-2 variants, reaching a 20 fM detection limit—over 100× better than glass[199]. Zhu and co-workers then introduced in-frame gold-nanoparticle arrays paired with microplate readers to quantify nucleocapsid protein at 44 fg·mL^{-1} within 3 min, and, with single-molecule counting, pushed sensitivity to 0.84 ag·mL^{-1} [200]. These breakthroughs highlight SEF's transformative role in rapid, ultrasensitive pathogen detection for disease monitoring and control.

 doi:10.20944/preprints202506.0169.v1

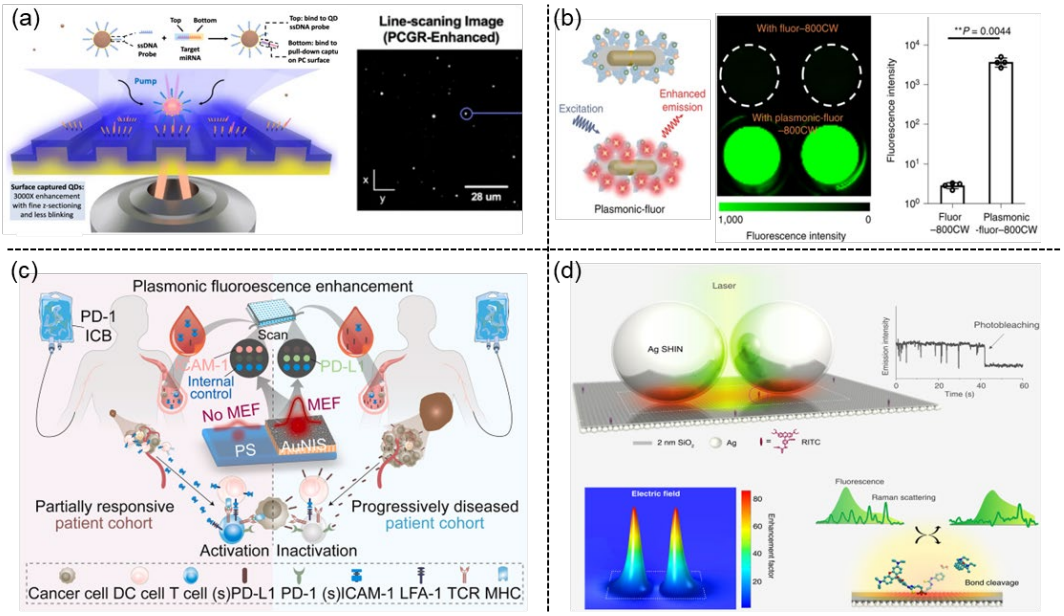

Figure 7. SEF-based sensing applications. (a) Single quantum dot digital resolution biosensing[40]. (b) Ultrabright fluorescent sensors for the femtomolar detection of analytes[190]. (c) A near-infrared fluorescence-enhanced plasmonic biosensing microarray[191]. (d) Real-time detection of single-molecule reaction by plasmon-enhanced spectroscopy[194].

4. Photonic Integrated Circuits and In-Sensor Computing

4.1. Photonic Integrated Circuits (PICs)

The rapid downsizing of electronic components to the submicron scale has brought about remarkable increases in computing power, coupled with significant cost reductions. As the microelectronics industry continues its journey towards smaller devices, it becomes increasingly plausible that both physical and economic constraints associated with top-down silicon technology will soon impose limitations on further progress. To overcome these limitations and meet the anticipated demands of future society, revolutionary breakthroughs, rather than incremental advances, are imperative. A promising avenue involves a paradigm shift from electronic signals to light. However, utilizing electromagnetic waves as information carriers in optical signal-processing devices and integrated circuits faces a formidable challenge – the limited integration and miniaturization available. This challenge is intricately linked to the diffraction limit of light in dielectric media, preventing the confinement of electromagnetic waves into nanoscale regions significantly smaller than the wavelength of light. Addressing this issue requires innovative approaches, and one captivating method involves leveraging the unique properties of plasmonic nanomaterials. Consequently, proposals for photonic components and electronic circuits based on localized plasmonic resonance have surfaced, demonstrating potential in tackling the scalability and performance challenges associated with future plasmonic integrated circuits (**Figure 8a**). This approach holds the promise of achieving all-optical processing of optical signals, thereby enhancing speed, bandwidth, and the overall capacity of information technology. Simultaneously, it presents an opportunity to reduce costs and power consumption, aligning with the evolving needs of future communication, computing, sensing, and other fields. This section provides an overview of recent strides in integrated electronic circuits grounded in plasmonic properties, encompassing plasmonic lasers, plasmonic gates, plasmonic modulators, plasmonic detectors, and plasmonic switches.

Optical logic gates are a part of the field of optical computing, which utilizes the principles of optics and photonics to manipulate light and perform logical operations similar to their electronic counterparts. *Fang* and colleagues reported a new method of optical modulation and logic based on organic/metal nanowire heterojunctions[201]. By coupling exciton polaritons in organic nanowires and surface plasmons in metal nanowires, the intensity of the output signal can be modulated (**Figure**

 doi:10.20944/preprints202506.0169.v1

8b). The organic/metal nanowire heterojunctions are selectively grown on the end of silver nanowires by physical vapor transport (**Figure 8b-I,II**). By changing the polarization direction of the incident laser, the absorption coefficient of the organic nanowire is adjusted, which affects the number of exciton polaritons in the organic nanowire and thus the intensity of the surface plasmons excited at the heterojunction, ultimately achieving modulation of the output signal intensity of the metal nanowire. 1 and 0 are defined according to the intensity of scattered plasmons. These four images (**Figure 8b-III-VI**) represent the four combinations of Boolean logic inputs: (1, 1), (1, 0), (0, 1), and (0, 0). In essence, a basic logic gate comprises two input ports (I1 and I2) and one output port (O). The gate's functionality is determined by the scattered plasmon intensity at the O port under varying input conditions (**Figure 8b-VII**). Utilizing an intensity threshold, such as 0.4 au (T1), enables the realization of OR and AND logic operations. For instance, with the intensity threshold set at 0.4 au, (I1 = 1, I2 = 1) yields O = 1, (I1 = 1, I2 = 0) results in O = 1, and (I1 = 0, I2 = 1) produces O = 1, demonstrating the OR gate behavior.

As for the light source in photonic circuits, it is required to be tunable and miniaturized. The Burstein-Moss (BM) effect is a phenomenon in which the apparent band gap of a semiconductor is increased as the absorption edge is pushed to higher energies as a result of some states close to the conduction band being populated. The BM effect has been used to realize lasers by increasing the carrier concentration in the semiconductor material, which in turn increases the population of electrons in the conduction band. For instance, *Liu* and colleagues reported on a novel method to tune the lasing wavelength of a single semiconductor nanowire by using the plasmon-enhanced BM effect (**Figure 8c**)[202]. The hybrid device consists of a single CdS nanowire placed on a thin SiO_2 layer over a Au film (**Figure 8c-I**). By varying the thickness of the SiO_2 layer, the coupling strength between the plasmons and the excitons is controlled, and thus the magnitude of the BM shift. They demonstrated that the lasing wavelength of the CdS nanowire laser can be tuned from 504 nm to 483 nm at room temperature by using the plasmon-enhanced BM effect. They also showed that the PL intensity and decay rate of the CdS nanowire are increased by the plasmonic coupling, indicating enhanced quantum efficiency.

Modulators in photonic circuits are also required to be miniaturized. Resonant modulators can be very compact. a device with a footprint as small as 78 μm^2 has already been demonstrated [203]. Plasmon can further miniaturize the resonant device size. *Melikyan* and colleagues developed a high-speed plasmonic phase modulator (PPM) that can encode information in the phase of surface plasmon polaritons at a bit rate of 40 Gbit s^{-1} and the device length is only 29 μm (**Figure 8d**) [204]. The PPM consists of two metal tapers that perform the photonic-to-plasmonic mode conversion and a phase modulator section located between them (**Figure 8d-I**). The metal taper narrows with an angle of 15° and is used as an interface between the silicon photonics and plasmonics. Light guided through the silicon nanowire efficiently excites the plasmonic resonant via the metal taper. The plasmonic resonance is then guided into the phase modulator section, which consists of two metal pads separated horizontally by a nanometre-scale vertical slot. The slot is filled with a nonlinear organic material, the refractive index n of which can be changed via the Pockels effect by applying a static electric field U/w_{gap} (modulating voltage U, gap width w_{gap}). By modulating the refractive index of the polymer in the slot, the information is encoded in the phase of the plasmonic resonance. At the end of the modulator section, the plasmonic resonance is back-converted into a photonic mode. With appropriate lumped elements (**Figure 8d-II**), the PPM operates across a 120-nm-wide wavelength range centred at 1,550 nm. It also has a flat modulation frequency response up to at least 65 GHz and a thermal stability up to 85 °C.

In terms of plasmonic detectors, the issues mainly focus on ohmic losses and integration challenge. First, the plasmonic signals are attenuated by the scattering and absorption of electrons in the metal layers, limiting the signal transfer distances to the sub-centimeter range. Then, the plasmonic detector needs to be compatible with electronic and photonic circuits, and to overcome the size mismatch between the plasmonic modes and the conventional optical modes. One promising solution is the integration of a metal–insulator–metal (MIM) waveguide with an inherently fast

 doi:10.20944/preprints202506.0169.v1

nanoslit metal–semiconductor–metal (MSM) photodetector, as demonstrated by *Neutens* and colleagues (**Figure 8e-I**)[205]. The MSM detector acts as both a contact and a coupler for the plasmons. The detector has a very fast photoresponse and a high signal-to-noise ratio, making it suitable for high-bandwidth applications. According to the polarization-dependent and spectral measurements, the detector has a e^{-1} decay lengths of 3.5 μm for a free-space wavelength of 660 nm to 9.5 μm for 870 nm (**Figure 8e-II**).

The primary function of an optical switcher is to selectively route optical signals from one input port to one or more output ports. Plasmonic optical switchers leverage the unique properties of plasmonic materials to provide advantages such as subwavelength-scale operation, high-speed performance, enhanced light-matter interaction, integration with electronics, miniaturization, tunable properties, and potentially lower energy consumption. These devices operate on the nanoscale, enabling compact and efficient optical circuits, while their rapid response to surface plasmon resonances supports ultrafast switching for applications requiring high-speed data transmission. Additionally, the tunability of plasmonic materials and their integration with electronic components contribute to the adaptability and versatility of these optical switchers. For instance, the resonance coupling between gold nanorods and photochromic dye molecules can be used to switch the light, as demonstrated by *Ming* and colleagues (**Figure 8f**)[206]. The switch consists of gold nanorods deposited on glass slides, coated with mesostructured silica thin films containing photochromic dye molecules. The structure is designed to enable plasmonic-molecular resonance coupling. The switch operates by monitoring the scattered light from single gold nanorods. UV light illumination induces a reversible change in the dye molecules, which affects the plasmon resonance wavelength and intensity, enabling the switching action (**Figure 8f-I,II**). The modulation depth of the resonance coupling-based single-nanorod plasmonic switch reaches 7.2 dB, and the number of the photochromic molecules that are actively involved in the switching process is estimated to be ~17000. The estimated laser power and energy required for operating a single-nanorod plasmonic switch are ~13 pW and ~39 pJ, respectively.

 doi:10.20944/preprints202506.0169.v1

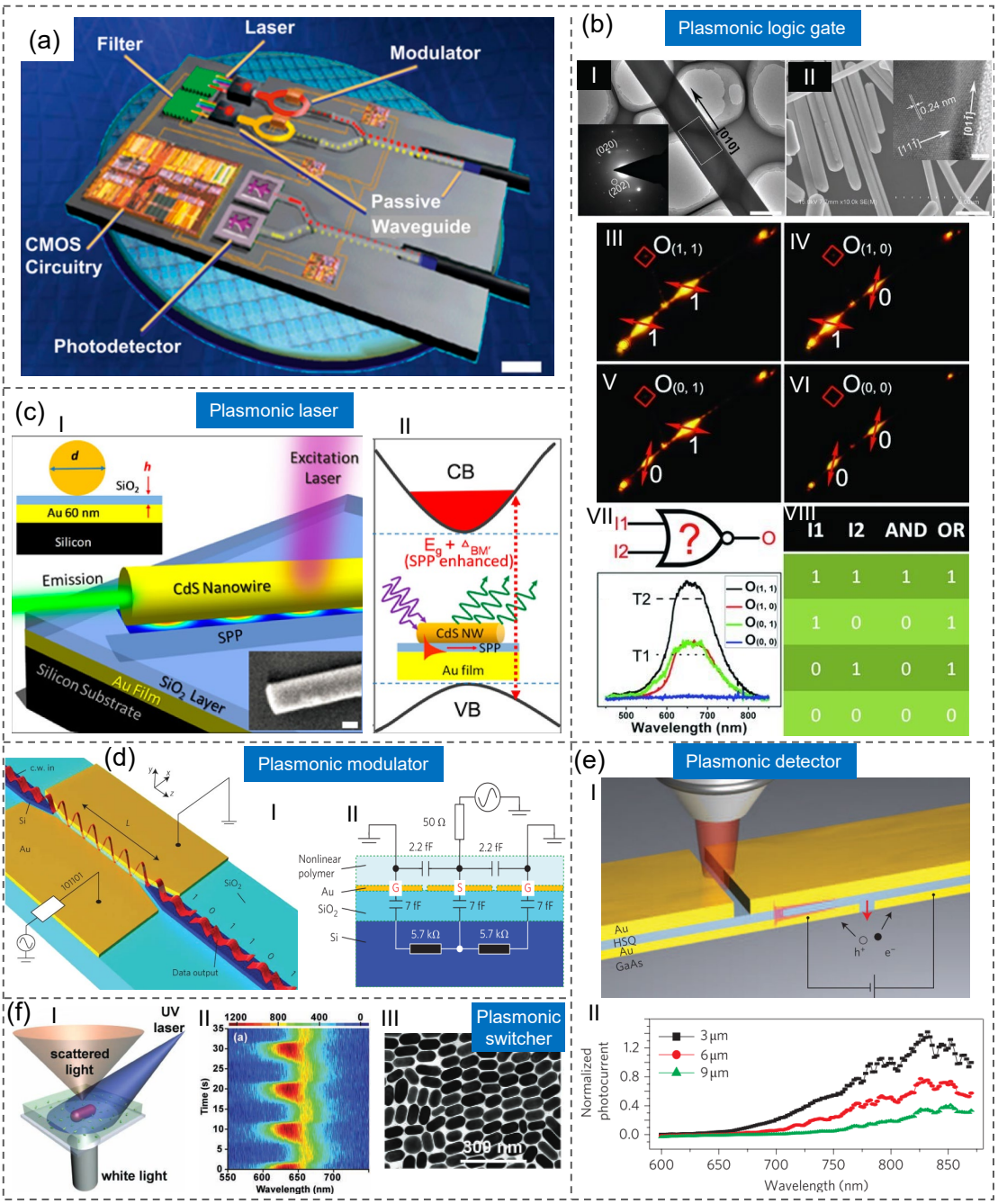

Figure 8. Integrated plasmonic circuits. (a) Overview of plasmonic integrated circuit components featuring high functionality on small wafer footprints[207]. (b) Plasmonic logic gates as basic components of digital circuits[201]. I: TEM image of the device. II: SEM image. III-VI: Photoluminescence microscopy images using four distinct combinations of polarized inputs. The polarisation directions of the two laser beams are denoted by red arrows. The values 1 and 0 were assigned based on the intensities of the scattered surface plasmon polaritons. VII, VIII: A fundamental logic gate featuring dual inputs and a single output signal is constructed. The optical logic operations, encompassing AND and OR gates, are succinctly summarized, along with the scattering spectra of plasmons at the O-terminal under excitations denoted in (III-VI). T1 and T2 denote the thresholds for the OR and AND gates, respectively. (c) Plasmonic laser as a nanolight source[202]. I: Schematic representation of the laser. II: Working mechanism. (d) Plasmonic modulator as an adaptor[204]. I: Schematic representation of the modulator. II: Lumped element model of the modulator. (e) Plasmonic detector as an interface to an electric circuit[205]. I: Schematic representation of the detector. II: Spectral responses of the detectors. (f) Plasmonic switcher[206]. I: A schematic illustration depicting a plasmonic switch that operates through resonance coupling between a solitary gold nanorod and photochromic dye molecules. II: Contour plot showing the on-off switching. III: TEM image of the plasmonic nanorod.

 doi:10.20944/preprints202506.0169.v1

4.2. In-Sensor Computing

As sensors become more advanced and numerous, the challenge is no longer just detecting a signal, but making sense of overwhelming amounts of data in real time. This is where the concept of in-sensor computing comes into play – blurring the boundary between sensing and computing. In traditional systems, a sensor captures data (e.g. an analog optical signal), which is then digitized and sent to a separate processor (CPU/GPU or cloud server) for analysis. This paradigm faces bottlenecks, especially for high-bandwidth data like images or spectra, because of the latency and energy cost of transferring data and performing electronic processing. In-sensor computing instead aims to perform initial processing or even full pattern recognition within the sensor hardware, before the data is fully digitized or transmitted. In other words, the sensor itself becomes a primitive computer, executing, for example, feature extraction or neural network inference on the analog signals it receives.

Photonic integrated circuits offer exciting opportunities for in-sensor computing because they can potentially handle computations at the speed of light with low latency. One approach uses the physics of the photonic device to compute a function of the input. For example, a network of interferometers can multiply and accumulate optical signals, effectively acting as an analog linear algebra engine (useful for neural network operations). Specifically, Liu *et al.* present a silicon-on-insulator mid-infrared (MIR) waveguide platform that not only functions as a high-sensitivity "photonic nose" for volatile organic compound (VOC) detection, but also exemplifies the emerging paradigm of in-sensor computing by tightly coupling on-chip light–matter interaction with machine-learning inference (**Figure 9a**). By designing a suspended spiral waveguide clad with subwavelength-grating (SWG) support structures, they achieve both low propagation loss—by removing the underlying oxide layer—and an exceptionally large external confinement factor (up to 85.9%), which directly enhances the evanescent-field interaction length with analytes. Finite-difference-time-domain simulations guided the optimization of SWG period and duty cycle, yielding a figure of merit (ratio of confinement factor to loss) of 0.77, a balance critical for maximizing sensitivity without incurring prohibitive attenuation. Experimentally, the platform demonstrates rapid, linear responses to single-component gases: for isopropyl alcohol (IPA) and acetone, absorbance scales linearly across a wide range of concentrations (up to 95% of each gas's lower explosion limit), with response times under 4 s and limits of detection near 200 ppm after 34 s of averaging. These results validate the waveguide's ability to faithfully transduce molecular absorption into optical intensity changes at high speed, a prerequisite for edge-based sensor analytics. To realize in-sensor computing capabilities, they integrate two machine-learning models into their sensing workflow. A one-dimensional convolutional neural network (1D-CNN) is trained on broadband MIR absorption spectra (3.65–3.80 μm) to classify 19 predefined binary mixing ratios of IPA and acetone, achieving 93.6% accuracy on unseen data. Beyond classification, a multilayer perceptron (MLP) regressor decomposes each mixture spectrum into its two pure-component spectra, enabling quantitative concentration predictions with an average root-mean-square error of 2.44 vol% across all mixtures.

Other approaches combine optoelectronic elements so that detection and weighting operations occur simultaneously; a recent demonstration showed a waveguide-integrated graphene photodetector whose responsivity can be tuned, thereby implementing a tunable weight for optical signals in a photonic computing architecture[208]. Specifically, Liu *et al.* introduce a fully waveguide-integrated photonic in-sensor computing unit that extends neuromorphic processing into the MIR domain, exploiting the rich molecular "fingerprints" present between 3.65 and 3.8 μm (**Figure 9b**). Fabricated on a standard silicon-on-insulator platform, the core of their design is a suspended silicon waveguide coupled to a few-layer graphene photodetector whose photoresponsivity can be tuned via an applied bias voltage. By patterning subwavelength-grating supports, they achieve both low propagation loss and a high external confinement factor, critical for maximizing light–matter interaction with analytes and for assuring sufficient optical power at the detector interface. The device's operational principle hinges on bias-controlled photoconductive gain: under a DC bias sweeping from −0.4 to +0.4 V, the graphene layer displays 16 clearly distinguishable responsivity states, equivalent to 4 bits of weighting precision. To validate the platform's versatility, three distinct

 doi:10.20944/preprints202506.0169.v1

neuromorphic tasks are executed entirely at the optical frontend. First, an array of four waveguide-photodetector channels implements 2 × 2 convolution kernels for edge detection on MNIST digit and fashion-item images. Second, the photodetector processes electronic resistive-sensor outputs for hand-gesture recognition. Here, five voltage signals from a resistive glove are mapped to bias voltages, while a constant optical input encodes learned weight patterns. Finally, leveraging the intrinsic spectral selectivity of the MIR waveguide, the authors perform gas-mixture classification in real time. A set of 19 binary mixtures of volatile organic compounds is spectrally encoded onto the waveguide, and individual detectors carry out weighted summation via bias tuning.

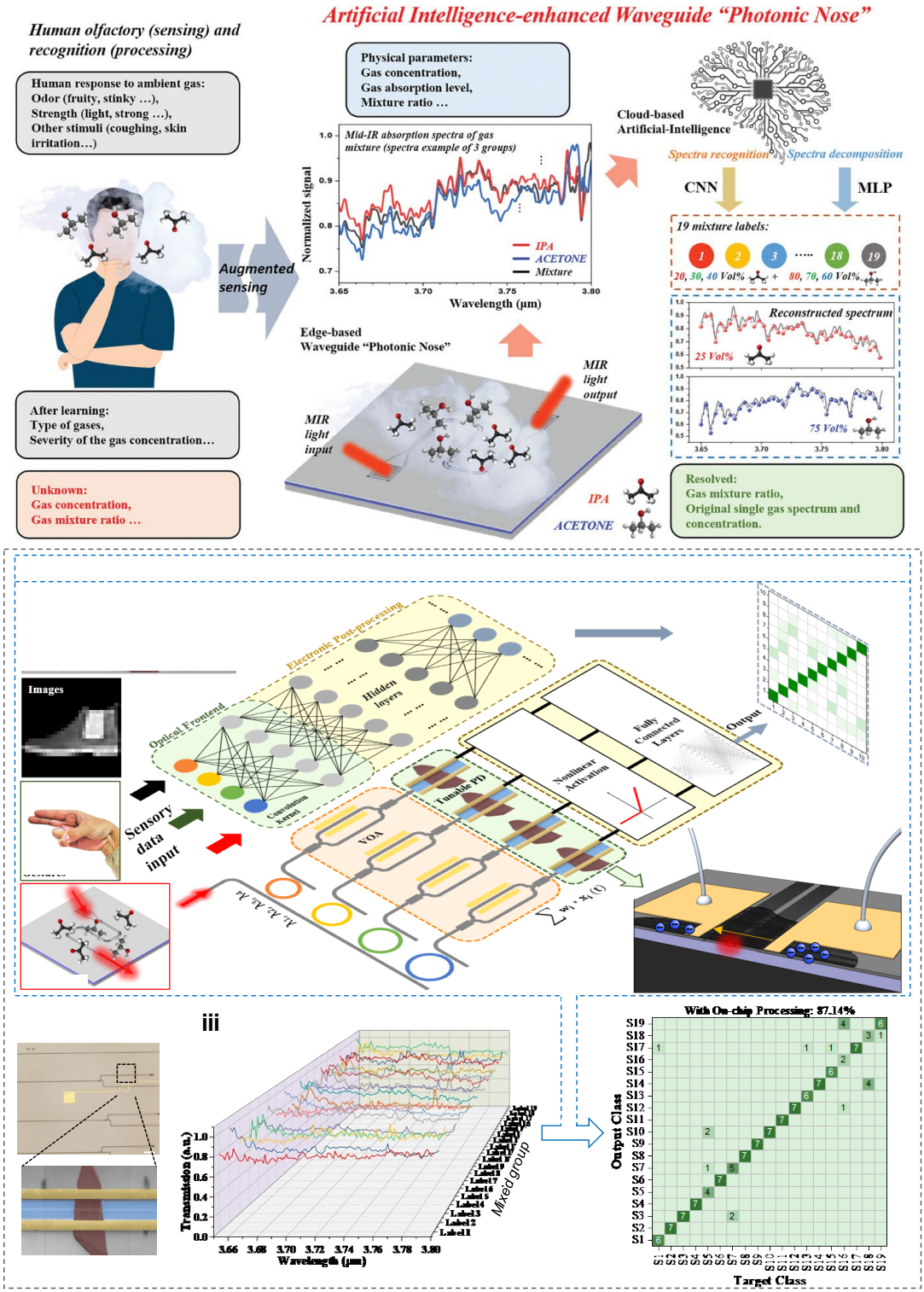

 doi:10.20944/preprints202506.0169.v1

Figure 9. Photonic integrated circuit-based sensors. (a) AI-enhanced mid-infrared photonic waveguide sensor for gas-mixture detection[209]. Analogous to the human olfactory system, where receptors transduce odorants and the brain interprets identity and strength, this edge-based "photonic nose" acquires absorption spectra, and a cloud-based machine-learning model infers component identities and concentrations. (b) Waveguide-integrated mid-infrared optoelectronic processing unit[208]. Mid-IR light is split into multiple waveguide channels, each encoding a sensory signal. A bias-tunable graphene photodetector multiplies these optical signals, which are then summed and forwarded to an electrical post-processor for classification.

In addition to single in-sensor computing, hybrid near-sensor edge computing system shows more possibilities. For instance, Ren *et al.* reported a fully integrated "near-sensor edge computing" (NSEC) platform built on a CMOS-compatible bilayer aluminum nitride/silicon (AlN/Si) photonic integrated circuit (**Figure 10**). The system cleverly combines two complementary photonic building blocks—AlN microring resonators (MRRs) for feature extraction and Si Mach–Zehnder interferometers (MZIs) for neural-network–style weighting—in a compact chip, enabling real-time, low-power AI at the sensor edge. Fabricated on an 8-inch silicon-on-insulator wafer with a 220 nm Si device layer, the process proceeds through deep-UV lithography, etching, SiO_2 planarization, AlN deposition, and precise patterning of both AlN and Si layers to form a dual-layer waveguide. Inter-layer adiabatic couplers achieve ultra-broadband, low-loss (0.04 dB per transition) coupling between Si and AlN, while AlN MRRs exhibit a DC tuning efficiency of 0.26 pm V^{-1} via the Pockels effect. The Si MZIs, equipped with TiN microheaters, realize a 30 dB modulation depth with $V\pi \approx 5.6$ V. Together, these photonic components sustain high optical quality ($Q \approx 65\,700$ for MRRs) and precise phase control, laying the hardware foundation for on-chip photonic computing.

In the first "feature-extraction" phase, contact-separation triboelectric nanogenerator (TENG) sensors mounted on gloves and socks serve as self-powered electrical inputs. The TENG outputs—spike-like voltages proportional to applied force—drive the AlN MRRs, which integrate the input over time (equivalent to an optical integrator) and map continuous mechanical dynamics onto the resonance-shifted optical output. For glove-based gesture recognition, four MRR channels capture bending at the thumb and three fingers, and a simple fully connected neural network trained on these photonic features attains 100 % accuracy over 13 American-Sign-Language gestures. Similarly, four TENG sensors in socks, placed under the forefoot and heel, produce resonance shifts up to 18 pm under 50–800 N loads; sampling at an optimal probe wavelength yields seven gait-cycle states that a neural network classifies with 99 % accuracy

Phase 2 integrates the photonic feature extractor with a 4 × 4 photonic neural network (PNN) on the same chip. Four parallel laser paths feed the MRRs, whose outputs enter the Si MZI array. By applying precise voltages to the thermo-optic heaters, the MZIs implement matrix–vector multiplications in the optical domain; outputs are combined and photodetected for digital nonlinear activation and backpropagation during training. Detailed noise characterization—0.02 SD for MRRs and 0.016 SD for MZIs—reveals Gaussian distributions, enabling a 4-bit quantization scheme that aligns weight states above the noise floor. Under this scheme, the on-chip PNN achieves 96.77 % accuracy for real-time glove-gesture inference and 98.31 % for sock-gait analysis, compared to 74.56 % and 59.2 % in the unquantized analog case.

Beyond these demos, the authors envision mixed-reality and metaverse applications: low-latency (< 10 ns), ultra-low-energy (< 0.34 pJ per inference) photonic AI interfaces for VR/AR control and fall detection, all executed on-chip without cloud dependence.

 doi:10.20944/preprints202506.0169.v1

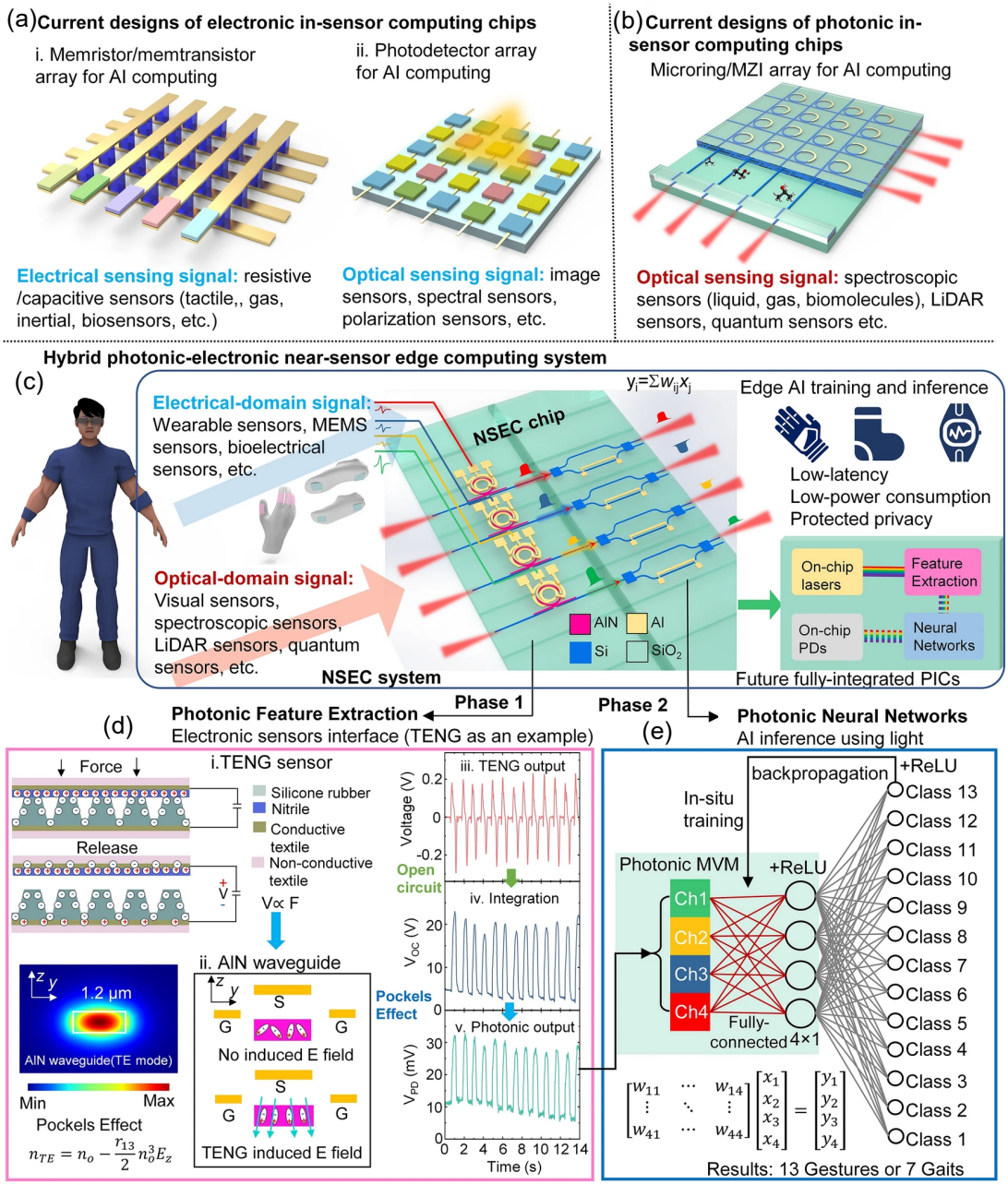

Figure 10. Photonic integrated circuit-based sensors. (a) AI-enhanced mid-infrared photonic waveguide sensor for gas-mixture detection[209]. Analogous to the human olfactory system, where receptors transduce odorants and the brain interprets identity and strength, this edge-based "photonic nose" acquires absorption spectra, and a cloud-based machine-learning model infers component identities and concentrations. (b) Waveguide-integrated mid-infrared optoelectronic processing unit[208]. Mid-IR light is split into multiple waveguide channels, each encoding a sensory signal. A bias-tunable graphene photodetector multiplies these optical signals, which are then summed and forwarded to an electrical post-processor for classification.

5. Challenges, Conclusions and Outlook

5.1. Challenges

While the progress in PIC sensors and AI-driven sensing is impressive, several challenges remain on the road to fully autonomous, miniaturized intelligent sensors. Overcoming these barriers is the focus of intense research. In this section, we summarize key technological barriers and emerging research directions aimed at addressing them.

Integration complexity and packaging: Integrating diverse optical, electrical, and fluidic components on a single platform is non-trivial. Many cutting-edge sensors (like the bottle resonator

 doi:10.20944/preprints202506.0169.v1

example) still require hybrid assembly of parts with extremely tight tolerances. Aligning fibers or free-space optics to chips, integrating light sources (lasers) on-chip, and combining microfluidics for sample delivery are all challenges that can increase complexity and cost. Achieving *fully integrated* sensors (with on-chip light generation, sensing, and readout) is an ongoing goal. Packaging—the protective housing and interface of the chip with the outside world—can introduce losses or variability that degrade performance.

Materials and spectral coverage: The material platforms used in photonic integration each have limitations. For instance, silicon photonics (using silicon-on-insulator waveguides) works well in the near-infrared (around 1.3–1.55 μm) but silicon is opaque to visible wavelengths and much of the mid-infrared beyond ~8 μm. For sensing applications, different spectral bands are important: visible for fluorescence, mid-IR for molecular absorption, etc. Thus, new materials like silicon nitride (which can handle visible to near-IR) or chalcogenide glasses and germanium (for mid-IR) are being explored. Integrating active materials is also a challenge – silicon is not optically active (can't emit light efficiently), so adding lasers or amplifiers may require III-V semiconductors (InP, GaAs) bonded or co-grown on silicon. This heterogenous integration adds complexity. Moreover, many sensors benefit from functional materials (e.g. graphene, lithium niobate, piezoelectric films) to achieve tunability or higher performance.

Signal processing and data handling bottlenecks: As sensors become more sensitive and multi-modal, they generate larger volumes of data. A single spectroscopic sensor array or imaging sensor can produce a firehose of information. Transmitting this raw data to a central location for processing (or even just to the edge of the chip) can overwhelm bandwidth and power budgets. This is one motivation for in-sensor or near-sensor computing. However, implementing sophisticated processing on-chip is challenging. All-optical computing schemes, while ultrafast, are often limited in complexity or reconfigurability (it's non-trivial to implement deep neural networks purely with linear optics, and nonlinear optical processing is still primitive at chip-scale). Electronic co-processors on the sensor chip could pick up the slack, but integrating high-performance electronics with photonics has thermal and noise implications.

5.2. Conclusions and Outlook

This review has outlined the sensing principles and applications of optical microsystems, and show how these microsystems – whether based on refractive index shifts, vibrational spectroscopy, or fluorescence – provided the foundation of knowledge and techniques that PIC sensors build upon. By integrating these optical elements on-chip, we attain leaps in scalability and the possibility of pervasive deployment. The incorporation of AI and in-sensor computing is arguably as revolutionary as the hardware advances.

Looking forward, we anticipate several developments. First, many PIC sensors will transition from the lab to the field. Just as integrated electronics went from demonstration chips to ubiquitous devices, integrated photonic sensors will begin to appear in everyday objects. We may see disposable photonic biosensor chips in at-home test kits for health diagnostics, wearable optical sensors tracking metabolites or vital signs non-invasively, and smartphone-integrated spectrometers for things like food scanning or air quality checking. The cost per sensor is likely to drop as semiconductor fabs start producing them in large volumes, especially if standardization efforts bear fruit. Second, the synergy with AI will deepen. Rather than AI being an add-on (in the cloud or on a paired smartphone), future sensors might include specialized on-chip AI accelerators (perhaps optical ones) that make them intelligent at the core. We foresee "smart pixels" and "smart waveguides" – sensing elements that inherently perform computations like pattern recognition. This could blur the line between sensor and computer, giving rise to a class of devices that are both. Third, autonomy will be a defining feature. Powered by energy harvesting (solar, RF, or even powering via photonic power delivery through fiber), a sensor node could operate indefinitely, communicating wirelessly its high-level findings. Swarms of such sensors might continuously map environmental parameters, and networks

 doi:10.20944/preprints202506.0169.v1

of medical sensors might continuously keep track of a patient's health, with AI spotting anomalies and alerting in real-time.

Of course, realizing this vision requires continued interdisciplinary effort. Advances in material science will be needed to integrate new functionalities onto photonic chips. Progress in nanofabrication will dictate how complex and precise our PIC sensors can become (for instance, nanometer-scale features for plasmonics or sub-wavelength meta-optics on-chip). On the AI side, algorithms will need to be tailored to work with sensor hardware constraints – for example, developing neural network models that can run on analog optical hardware or be robust to the analog noise in sensor signals. There is also a significant role for system engineering: figuring out how to reliably package, power, network, and maintain thousands or millions of these sensors in the field. Issues like security (ensuring sensor data and decision-making are trustworthy) will also need attention as these devices become critical to infrastructure and personal healthcare.

Author Contributions: Conceptualization, H.Z. and D.L.; writing—original draft preparation, H.Z.; writing—review and editing, H.Z.; supervision, H.Z. and C.L.; project administration, H.Z.; funding acquisition, H.Z. All authors have read and agreed to the published version of the manuscript.

Funding: This research was funded by Fundamental Scientific Research Funds for Central Universities of China (Grant No. G2025KY05053).

Institutional Review Board Statement: Not applicable.

Informed Consent Statement: Not applicable.

Data Availability Statement: No new data were created or analyzed in this study. Data sharing is not applicable to this article.

Conflicts of Interest: The authors declare no conflicts of interest.

Abbreviations

The following abbreviations are used in this manuscript:

AI	Artificial Intelligence
PIC	Photonic integrated circuits
SEIRA	Surface-enhanced infrared absorption
RI	Refractive index
SERS	Surface-enhanced Raman spectroscopy
SEF	Surface enhanced fluorescence
CD	Circular dichroism
ELISA	Enzyme-linked immunosorbent assays
PSA	prostate-specific antigen
LSPR	Localized surface plasmon resonance

References

1. Zhou, H.; Li, D.; Lv, Q.; Lee, C., Integrative plasmonics: optical multi-effects and acousto-electric-thermal fusion for biosensing, energy conversion, and photonic circuits. *Chem. Soc. Rev.* **2025**.
2. Xiao, Z.; Liu, W.; Xu, S.; Zhou, J.; Ren, Z.; Lee, C., Recent Progress in Silicon-Based Photonic Integrated Circuits and Emerging Applications. *Adv. Opt. Mater.* **2023,** 11, 2301028.
3. Zhuge, Y.; Ren, Z.; Xiao, Z.; Zhang, Z.; Liu, X.; Liu, W.; Xu, S.; Ho, C. P.; Li, N.; Lee, C., Photonic Bayesian Neural Networks: Leveraging Programmable Noise for Robust and Uncertainty-Aware Computing. *Adv. Sci.* **2025**, e2500525.
4. Zhou, J.; Liu, X.; Zhou, H.; Xu, S.; Xie, J.; Xu, C.; Liu, W.; Zhang, Z.; Lee, C., Artificial-Intelligence-Enhanced Mid-infrared Lab-on-a-Chip for Mixture Spectroscopy Analysis. *Laser Photonics Rev.* **2024,** 19, 2400754.
5. Lialiou, P.; Maglogiannis, I., Students' Burnout Symptoms Detection Using Smartwatch Wearable Devices: A Systematic Literature Review. *AI Sensors* **2025,** 1.

 doi:10.20944/preprints202506.0169.v1

6. Zhou, H.; Xu, L.; Ren, Z.; Zhu, J.; Lee, C., Machine learning-augmented surface-enhanced spectroscopy toward next-generation molecular diagnostics. *Nanoscale Adv.* **2023,** 5, 538-570.
7. Wang, C.; He, T.; Zhou, H.; Zhang, Z.; Lee, C., Artificial intelligence enhanced sensors - enabling technologies to next-generation healthcare and biomedical platform. *Bioelectron. Med.* **2023,** 9, 17.
8. Zhou, H.; Li, D.; He, X.; Hui, X.; Guo, H.; Hu, C.; Mu, X.; Wang, Z. L., Bionic Ultra-Sensitive Self-Powered Electromechanical Sensor for Muscle-Triggered Communication Application. *Adv. Sci.* **2021,** 8, e2101020.
9. Zhang, Z.; Liu, X.; Zhou, H.; Xu, S.; Lee, C., Advances in Machine-Learning Enhanced Nanosensors: From Cloud Artificial Intelligence Toward Future Edge Computing at Chip Level. *Small Struct.* **2023,** 5, 2300325.
10. Dong, B.; Aggarwal, S.; Zhou, W.; Ali, U. E.; Farmakidis, N.; Lee, J. S.; He, Y.; Li, X.; Kwong, D.-L.; Wright, C. D.; Pernice, W. H. P.; Bhaskaran, H., Higher-dimensional processing using a photonic tensor core with continuous-time data. *Nat. Photonics* **2023**.
11. Sun, Z.; He, T.; Ren, Z.; Wang, C.; Liu, X.; Zhang, Z.; Zhou, J.; Guo, X.; Yang, Y.; Lee, C., Moving Toward Human-Like Perception and Sensation Systems—From Integrated Intelligent Systems to Decentralized Smart Devices. *SmartSys* **2025,** 1.
12. Janneh, M.; De Marcellis, A.; Palange, E.; Rizza, C.; Ciattoni, A.; Mengali, S., Modelling of Nanoantenna-Based Optical Sensors for High-Sensitivity High-Resolution Infrared Spectroscopy of Chemical Compounds. In *Sensors*, Compagnone, D.; Baldini, F.; DiNatale, C.; Betta, G.; Siciliano, P., Eds. 2015; Vol. 319, pp 109-113.
13. Lowry, T. W.; Prommapan, P.; Rainer, Q.; Van Winkle, D.; Lenhert, S., Lipid Multilayer Grating Arrays Integrated by Nanointaglio for Vapor Sensing by an Optical Nose. *Sensors* **2015,** 15, 20863-20872.
14. Swargiary, K.; Jitpratak, P.; Pathak, A. K.; Viphavakit, C., Low-Cost ZnO Spray-Coated Optical Fiber Sensor for Detecting VOC Biomarkers of Diabetes. *Sensors* **2023,** 23.
15. Zhou, H.; Yang, C.; Hu, D.; Li, D.; Hui, X.; Zhang, F.; Chen, M.; Mu, X., Terahertz biosensing based on bi-layer metamaterial absorbers toward ultra-high sensitivity and simple fabrication. *Appl. Phys. Lett.* **2019,** 115, 143507.
16. Zhou, H.; Yang, C.; Hu, D.; Dou, S.; Hui, X.; Zhang, F.; Chen, C.; Chen, M.; Yang, Y.; Mu, X., Integrating a Microwave Resonator and a Microchannel with an Immunochromatographic Strip for Stable and Quantitative Biodetection. *ACS Appl. Mater. Interfaces* **2019,** 11, 14630-14639.
17. Zhou, H.; Hu, D.; Yang, C.; Chen, C.; Ji, J.; Chen, M.; Chen, Y.; Yang, Y.; Mu, X., Multi-Band Sensing for Dielectric Property of Chemicals Using Metamaterial Integrated Microfluidic Sensor. *Sci. Rep.* **2018,** 8, 14801.
18. Walden, S. L.; Poudel, P.; Zou, C.; Tanaka, K.; Paul, P.; Szeghalmi, A.; Siefke, T.; Pertsch, T.; Schacher, F. H.; Staude, I., Two-Color Spatially Resolved Tuning of Polymer-Coated Metasurfaces. *ACS Nano* **2024,** 18, 5079-5088.
19. Luo, M.; Zhou, Y.; Zhao, X.; Guo, Z.; Li, Y.; Wang, Q.; Liu, J.; Luo, W.; Shi, Y.; Liu, A. Q.; Wu, X., High-sensitivity optical sensors empowered by quasi-bound states in the continuum in a hybrid metal-dielectric metasurface. *ACS Nano* **2024,** 18, 6477-6486.
20. Yang, Y. M.; Kravchenko, II; Briggs, D. P.; Valentine, J., All-dielectric metasurface analogue of electromagnetically induced transparency. *Nat. Commun.* **2014,** 5.
21. Spacková, B.; Wrobel, P.; Bocková, M.; Homola, J., Optical Biosensors Based on Plasmonic Nanostructures: A Review. *Proceedings of the Ieee* **2016,** 104, 2380-2408.
22. Otte, M. A.; Sepúlveda, B.; Ni, W. H.; Juste, J. P.; Liz-Marzán, L. M.; Lechuga, L. M., Identification of the Optimal Spectral Region for Plasmonic and Nanoplasmonic Sensing. *ACS Nano* **2010,** 4, 349-357.
23. Zhou, H.; Li, D.; Ren, Z.; Xu, C.; Wang, L.-F.; Lee, C., Surface plasmons-phonons for mid-infrared hyperspectral imaging. *Science Advances* **2024,** 10, eado3179.
24. Li, D.; Zhou, H.; Ren, Z.; Lee, C., Advances in MEMS, Optical MEMS, and Nanophotonics Technologies for Volatile Organic Compound Detection and Applications. *Small Sci.* **2024,** 5, 202400250.
25. Li, D.; Yadav, A.; Zhou, H.; Roy, K.; Thanasekaran, P.; Lee, C., Advances and Applications of Metal-Organic Frameworks (MOFs) in Emerging Technologies: A Comprehensive Review. *Glob. Chall.* **2024,** 8, 2300244.
26. Miao, X. L.; Luk, T. S.; Liu, P. Q., Liquid-Metal-Based Nanophotonic Structures for High-Performance SEIRA Sensing. *Adv. Mater.* **2022,** 34.

 doi:10.20944/preprints202506.0169.v1

27. Wagner, M.; Seifert, A.; Liz-Marzan, L. M., Towards multi-molecular surface-enhanced infrared absorption using metal plasmonics. *Nanoscale Horiz.* **2022,** 7, 1259-1278.
28. Kozuch, J.; Ataka, K.; Heberle, J., Surface-enhanced infrared absorption spectroscopy. *Nat. Rev. Methods Primers* **2023,** 3.
29. Chen, C.; Liu, W.; Tian, S.; Hong, T., Novel Surface-Enhanced Raman Spectroscopy Techniques for DNA, Protein and Drug Detection. *Sensors* **2019,** 19.
30. Mondol, A. S.; Patel, M. D.; Ruger, J.; Stiebing, C.; Kleiber, A.; Henkel, T.; Popp, J.; Schie, I. W., Application of High-Throughput Screening Raman Spectroscopy (HTS-RS) for Label-Free Identification and Molecular Characterization of Pollen. *Sensors* **2019,** 19.
31. Park, S.; Lee, J.; Khan, S.; Wahab, A.; Kim, M., Machine Learning-Based Heavy Metal Ion Detection Using Surface-Enhanced Raman Spectroscopy. *Sensors* **2022,** 22.
32. Xu, X.; Zhang, W.-Y.; Ma, X.-Y.; Qin, X.; Jiang, T.-W.; Li, H.; Zhang, Y.; Jiang, K.; Cai, W.-B., Toward hyphenated in situ infrared and Raman spectroscopies in interfacial electrochemistry. *Anal. Chem.* **2025,** 97, 1047-1053.
33. Martens, R. R.; Gozdzialski, L.; Newman, E.; Gill, C.; Wallace, B.; Hore, D. K., Optimized machine learning approaches to combine surface-enhanced Raman scattering and infrared data for trace detection of xylazine in illicit opioids. *Analyst* **2025,** 150, 700-711.
34. Kang, H.; Lee, J.; Moon, J.; Lee, T.; Kim, J.; Jeong, Y.; Lim, E. K.; Jung, J.; Jung, Y.; Lee, S. J.; Lee, K. G.; Ryu, S.; Kang, T., Multiplex Detection of Foodborne Pathogens using 3D Nanostructure Swab and Deep Learning-Based Classification of Raman Spectra. *Small* **2024**, e2308317.
35. Yang, G.; Sun, L.; Zhang, Q., Multicomponent chiral plasmonic hybrid nanomaterials: recent advances in synthesis and applications. *Nanoscale Adv.* **2024,** 6, 318-336.
36. Li, H.; Ren, Y.; He, M.; Qi, H., Nanoparticle manipulation based on chiral plasmon effects. *Phys Chem Chem Phys* **2024,** 26, 17860-17868.
37. Biswas, A.; Cencillo-Abad, P.; Shabbir, M. W.; Karmakar, M.; Chanda, D., Tunable plasmonic superchiral light for ultrasensitive detection of chiral molecules. *Sci. Adv.* **2024,** 10, eadk2560.
38. He, P.; Li, W.; Ji, H.; Chang, H.; Yu, Y., Supercritical-lens light-sheet fluorescence microscopy with sub-diffraction-limit axial resolution, enhanced FOV, and chip-scale illumination. *Opt. Express* **2025,** 33, 10563-10573.
39. Zhang, S.; Fan, D.; Yan, Q.; Lu, Y.; Wu, D.; Fu, B.; Zhao, M., Single-molecule fluorescence imaging of photocatalytic nanomaterials. *J. Mater. Chem. A* **2024,** 12, 19627-19662.
40. Xiong, Y.; Huang, Q.; Canady, T. D.; Barya, P.; Liu, S.; Arogundade, O. H.; Race, C. M.; Che, C.; Wang, X.; Zhou, L.; Wang, X.; Kohli, M.; Smith, A. M.; Cunningham, B. T., Photonic crystal enhanced fluorescence emission and blinking suppression for single quantum dot digital resolution biosensing. *Nat. Commun.* **2022,** 13.
41. Fernández-Sánchez, C.; McNeil, C. J.; Rawson, K.; Nilsson, O.; Leung, H. Y.; Gnanapragasam, V., One-step immunostrip test for the simultaneous detection of free and total prostate specific antigen in serum. *J. Immunol. Methods* **2005,** 307, 1-12.
42. Mikolajczyk, S. D.; Catalona, W. J.; Evans, C. L.; Linton, H. J.; Millar, L. S.; Marker, K. M.; Katir, D.; Amirkhan, A.; Rittenhouse, H. G., Proenzyme forms of prostate-specific antigen in serum improve the detection of prostate cancer. *Clin. Chem.* **2004,** 50, 1017-1025.
43. Khan, Y.; Li, A.; Chang, L.; Li, L.; Guo, L., Gold nano disks arrays for localized surface plasmon resonance based detection of PSA cancer marker. *Sensors and Actuators B: Chemical* **2018,** 255, 1298-1307.
44. Théry, C.; Ostrowski, M.; Segura, E., Membrane vesicles as conveyors of immune responses. *Nat. Rev. Immunol.* **2009,** 9, 581-593.
45. Colombo, M.; Raposo, G.; Théry, C., Biogenesis, Secretion, and Intercellular Interactions of Exosomes and Other Extracellular Vesicles. In *Annual Review of Cell and Developmental Biology, Vol 30*, Schekman, R.; Lehmann, R., Eds. 2014; Vol. 30, pp 255-289.
46. Simpson, R. J.; Lim, J. W. E.; Moritz, R. L.; Mathivanan, S., Exosomes: proteomic insights and diagnostic potential. *Expert Rev. Proteomics* **2009,** 6, 267-283.

 doi:10.20944/preprints202506.0169.v1

47. Shao, H. L.; Im, H.; Castro, C. M.; Breakefield, X.; Weissleder, R.; Lee, H. H., New Technologies for Analysis of Extracellular Vesicles. *Chem. Rev.* **2018,** 118, 1917-1950.
48. El Andaloussi, S.; Maeger, I.; Breakefield, X. O.; Wood, M. J. A., Extracellular vesicles: biology and emerging therapeutic opportunities. *Nat. Rev. Drug Discovery* **2013,** 12, 348-358.
49. Wang, C. Y.; Huang, C. H.; Gao, Z. Q.; Shen, J. L.; He, J. C.; MacLachlan, A.; Ma, C.; Chang, Y.; Yang, W.; Cai, Y. X.; Lou, Y.; Dai, S. Y.; Chen, W. Q.; Li, F.; Chen, P. Y., Nanoplasmonic Sandwich Immunoassay for Tumor-Derived Exosome Detection and Exosomal PD-L1 Profiling. *Acs Sensors* **2021,** 6, 3308-3319.
50. Feng, H. T.; Min, S. Y.; Huang, Y. Q.; Gan, Z. F.; Liang, C. W.; Li, W. D.; Chen, Y., Concentric gradient nanoplasmonic sensors for detecting tumor-derived extracellular vesicles. *Sensors and Actuators B-Chemical* **2024,** 400.
51. Wang, Y. D.; Mao, Z. H.; Chen, Q.; Koh, K.; Hu, X. J.; Chen, H. X., Rapid and sensitive detection of PD-L1 exosomes using Cu-TCPP 2D MOF as a SPR sensitizer. *Biosens. Bioelectron.* **2022,** 201.
52. Théry, C.; Amigorena, S.; Raposo, G.; Clayton, A., Isolation and characterization of exosomes from cell culture supernatants and biological fluids. *Current protocols in cell biology* **2006,** 30, 3-22.
53. Im, H.; Shao, H.; Park, Y. I.; Peterson, V. M.; Castro, C. M.; Weissleder, R.; Lee, H., Label-free detection and molecular profiling of exosomes with a nano-plasmonic sensor. *Nat. Biotechnol.* **2014,** 32, 490-U219.
54. Lim, C. Z. J.; Zhang, Y.; Chen, Y.; Zhao, H. T.; Stephenson, M. C.; Ho, N. R. Y.; Chen, Y.; Chung, J.; Reilhac, A.; Loh, T. P.; Chen, C. L. H.; Shao, H. L., Subtyping of circulating exosome-bound amyloid beta reflects brain plaque deposition. *Nat. Commun.* **2019,** 10, 11.
55. Liu, L. H.; Iketani, S.; Guo, Y. C.; Chan, J. F. W.; Wang, M.; Liu, L. Y.; Luo, Y.; Chu, H.; Huang, Y. M.; Nair, M. S.; Yu, J.; Chik, K. K. H.; Yuen, T. T. T.; Yoon, C.; To, K. K. W.; Chen, H. L.; Yin, M. T.; Sobieszczyk, M. E.; Huang, Y. X.; Wang, H. H.; Sheng, Z. Z.; Yuen, K. Y.; Ho, D. D., Striking antibody evasion manifested by the Omicron variant of SARS-CoV-2. *Nature* **2022,** 602, 676-681.
56. Zhu, F. C.; Zhuang, C. L.; Chu, K.; Zhang, L.; Zhao, H.; Huang, S. J.; Su, Y. Y.; Lin, H. Y.; Yang, C. L.; Jiang, H. M.; Zang, X.; Liu, D. L.; Pan, H. X.; Hu, Y. M.; Liu, X. H.; Chen, Q.; Song, Q. Q.; Quan, J. L.; Huang, Z. H.; Zhong, G. H.; Chen, J. Y.; Han, J. L.; Sun, H.; Cui, L. B.; Li, J. X.; Chen, Y. X.; Zhang, T. Y.; Ye, X. Z.; Li, C. G.; Wu, T.; Zhang, J.; Xia, N. S., Safety and immunogenicity of a live-attenuated influenza virus vector-based intranasal SARS-CoV-2 vaccine in adults: randomised, double-blind, placebo-controlled, phase 1 and 2 trials. *Lancet Respiratory Medicine* **2022,** 10, 749-760.
57. Asghari, A.; Wang, C.; Yoo, K. M.; Rostamian, A.; Xu, X. C.; Shin, J. D.; Dalir, H.; Chen, R. T., Fast, accurate, point-of-care COVID-19 pandemic diagnosis enabled through advanced lab-on-chip optical biosensors: Opportunities and challenges. *Applied Physics Reviews* **2021,** 8.
58. Tan, X. T.; Krel, M.; Dolgov, E.; Park, S.; Li, X. Z.; Wu, W. S.; Sun, Y. L.; Zhang, J.; Oo, M. K. K.; Perlin, D. S.; Fan, X. D., Rapid and quantitative detection of SARS-CoV-2 specific IgG for convalescent serum evaluation. *Biosens. Bioelectron.* **2020,** 169.
59. Ogata, A. F.; Maley, A. M.; Wu, C.; Gilboa, T.; Norman, M.; Lazarovits, R.; Mao, C. P.; Newton, G.; Chang, M.; Nguyen, K.; Kamkaew, M.; Zhu, Q.; Gibson, T. E.; Ryan, E. T.; Charles, R. C.; Marasco, W. A.; Walt, D. R., Ultra-Sensitive Serial Profiling of SARS-CoV-2 Antigens and Antibodies in Plasma to Understand Disease Progression in COVID-19 Patients with Severe Disease. *Clin. Chem.* **2020,** 66, 1562-1572.
60. Li, F. J.; Hong, J. P.; Guan, C. H.; Chen, K. Y.; Xie, Y. N.; Wu, Q.; Chen, J. J.; Deng, B. C.; Shen, J. Q.; Liu, X. Y.; Hu, R. S.; Zhang, Y. L.; Chen, Y. X.; Zhu, J. F., Affinity Exploration of SARS-CoV-2 RBD Variants to mAb-Functionalized Plasmonic Metasurfaces for Label-Free Immunoassay Boosting. *ACS Nano* **2023**.
61. Yang, Y. J.; Murray, J.; Haverstick, J.; Tripp, R. A.; Zhao, Y. P., Silver nanotriangle array based LSPR sensor for rapid coronavirus detection. *Sensors and Actuators B-Chemical* **2022,** 359.
62. Funari, R.; Fukuyama, H.; Shen, A. Q., Nanoplasmonic multiplex biosensing for COVID-19 vaccines. *Biosens. Bioelectron.* **2022,** 208.
63. Huang, L. P.; Ding, L. F.; Zhou, J.; Chen, S. L.; Chen, F.; Zhao, C.; Xu, J. Q.; Hu, W. J.; Ji, J. S.; Xu, H.; Liu, G. L., One-step rapid quantification of SARS-CoV-2 virus particles via low-cost nanoplasmonic sensors in generic microplate reader and point-of-care device. *Biosens. Bioelectron.* **2021,** 171.
64. Funari, R.; Chu, K. Y.; Shen, A. Q., Detection of antibodies against SARS-CoV-2 spike protein by gold nanospikes in an opto-microfluidic chip. *Biosens. Bioelectron.* **2020,** 169, 112578.

 doi:10.20944/preprints202506.0169.v1

65. Lin, H. Y.; Huang, C. H.; Lu, S. H.; Kuo, I. T.; Chau, L. K., Direct detection of orchid viruses using nanorod-based fiber optic particle plasmon resonance immunosensor. *Biosens. Bioelectron.* **2014,** 51, 371-378.
66. Zheng, S.; Kim, D. K.; Park, T. J.; Lee, S. J.; Lee, S. Y., Label-free optical diagnosis of hepatitis B virus with genetically engineered fusion proteins. *Talanta* **2010,** 82, 803-809.
67. Yanik, A. A.; Huang, M.; Kamohara, O.; Artar, A.; Geisbert, T. W.; Connor, J. H.; Altug, H., An Optofluidic Nanoplasmonic Biosensor for Direct Detection of Live Viruses from Biological Media. *Nano Lett.* **2010,** 10, 4962-4969.
68. Yesilkoy, F.; Arvelo, E. R.; Jahani, Y.; Liu, M.; Tittl, A.; Cevher, V.; Kivshar, Y.; Altug, H., Ultrasensitive hyperspectral imaging and biodetection enabled by dielectric metasurfaces. *Nat. Photonics* **2019,** 13, 390-396.
69. Jahani, Y.; Arvelo, E. R.; Yesilkoy, F.; Koshelev, K.; Cianciaruso, C.; De Palma, M.; Kivshar, Y.; Altug, H., Imaging-based spectrometer-less optofluidic biosensors based on dielectric metasurfaces for detecting extracellular vesicles. *Nat. Commun.* **2021,** 12, 3246.
70. Khan, S. A.; Khan, N. Z.; Xie, Y. N.; Abbas, M. T.; Rauf, M.; Mehmood, I.; Runowski, M.; Agathopoulos, S.; Zhu, J. F., Optical Sensing by Metamaterials and Metasurfaces: From Physics to Biomolecule Detection. *Adv. Opt. Mater.* **2022,** 10.
71. Min, S.; Li, S.; Zhu, Z.; Liu, Y.; Liang, C.; Cai, J.; Han, F.; Li, Y.; Cai, W.; Cheng, X.; Li, W. D., Ultrasensitive Molecular Detection by Imaging of Centimeter-Scale Metasurfaces with a Deterministic Gradient Geometry. *Adv. Mater.* **2021,** 33, e2100270.
72. Wu, M.; Li, G.; Ye, X.; Zhou, B.; Zhou, J.; Cai, J., Ultrasensitive Molecular Detection at Subpicomolar Concentrations by the Diffraction Pattern Imaging with Plasmonic Metasurfaces and Convex Holographic Gratings. *Adv Sci (Weinh)* **2022,** 9, e2201682.
73. Wu, M. X.; Li, G. H.; Ye, X. Y.; Zhou, B.; Zhou, J. H.; Cai, J. X., Ultrasensitive Molecular Detection at Subpicomolar Concentrations by the Diffraction Pattern Imaging with Plasmonic Metasurfaces and Convex Holographic Gratings. *Adv. Sci.* **2022,** 9.
74. Ansaryan, S.; Liu, Y. C.; Li, X.; Economou, A. M.; Eberhardt, C. S.; Jandus, C.; Altug, H., High-throughput spatiotemporal monitoring of single-cell secretions via plasmonic microwell arrays. *Nat Biomed Eng* **2023**.
75. Shrivastav, A. M.; Mishra, S. K.; Gupta, B. D., Fiber optic SPR sensor for the detection of melamine using molecular imprinting. *Sensors and Actuators B-Chemical* **2015,** 212, 404-410.
76. Zhou, W. C.; Li, K. W.; Wei, Y. L.; Hao, P.; Chi, M. B.; Liu, Y. S.; Wu, Y. H., Ultrasensitive label-free optical microfiber coupler biosensor for detection of cardiac troponin I based on interference turning point effect. *Biosens. Bioelectron.* **2018,** 106, 99-104.
77. Huang, Y. Y.; Chen, P. W.; Liang, H.; Xiao, A. X.; Zeng, S. K.; Guan, B. O., Nucleic acid hybridization on a plasmonic nanointerface of optical microfiber enables ultrahigh-sensitive detection and potential photothermal therapy. *Biosens. Bioelectron.* **2020,** 156.
78. Chen, P. W.; Huang, Y. Y.; Bo, Y.; Liang, H.; Xiao, A. X.; Guan, B. O., 3D nanointerface enhanced optical microfiber for real-time detection and sizing of single nanoparticles. *Chem. Eng. J.* **2021,** 407.
79. Li, H. T.; Huang, Y. Y.; Hou, G. H.; Xiao, A. X.; Chen, P. W.; Liang, H.; Huang, Y. G.; Zhao, X. T.; Liang, L. L.; Feng, X. H.; Guan, B. O., Single-molecule detection of biomarker and localized cellular photothermal therapy using an optical microfiber with nanointerface. *Science Advances* **2019,** 5.
80. Huang, Y. Y.; Chen, P. W.; Zhou, L. Y.; Zheng, J. Y.; Wu, H. T.; Liang, J. X.; Xiao, A. X.; Li, J.; Guan, B. O., Plasmonic Coupling on an Optical Microfiber Surface: Enabling Single-Molecule and Noninvasive Dopamine Detection. *Adv. Mater.* **2023,** 35.
81. Raghunandhan, R.; Chen, L. H.; Long, H. Y.; Leam, L. L.; So, P. L.; Ning, X.; Chan, C. C., Chitosan/PAA based fiber-optic interferometric sensor for heavy metal ions detection. *Sensors and Actuators B-Chemical* **2016,** 233, 31-38.
82. Mariani, S.; Strambini, L. M.; Barillaro, G., Electrical Double Layer-Induced Ion Surface Accumulation for Ultrasensitive Refractive Index Sensing with Nanostructured Porous Silicon Interferometers. *Acs Sensors* **2018,** 3, 595-605.
83. Kim, K. J.; Lu, P.; Culp, J. T.; Ohodnicki, P. R., Metal-Organic Framework Thin Film Coated Optical Fiber Sensors: A Novel Waveguide-Based Chemical Sensing Platform. *Acs Sensors* **2018,** 3, 386-394.

 doi:10.20944/preprints202506.0169.v1

84. Ribaut, C.; Voisin, V.; Malachovská, V.; Dubois, V.; Mégret, P.; Wattiez, R.; Caucheteur, C., Small biomolecule immunosensing with plasmonic optical fiber grating sensor. *Biosens. Bioelectron.* **2016,** 77, 315-322.
85. Adato, R.; Altug, H., In-situ ultra-sensitive infrared absorption spectroscopy of biomolecule interactions in real time with plasmonic nanoantennas. *Nat. Commun.* **2013,** 4, 2154.
86. Ataka, K.; Kottke, T.; Heberle, J., Thinner, Smaller, Faster: IR Techniques To Probe the Functionality of Biological and Biomimetic Systems. *Angewandte Chemie-International Edition* **2010,** 49, 5416-5424.
87. Neubrech, F.; Huck, C.; Weber, K.; Pucci, A.; Giessen, H., Surface-Enhanced Infrared Spectroscopy Using Resonant Nanoantennas. *Chem. Rev.* **2017,** 117, 5110-5145.
88. Zhou, H.; Li, D. X.; Hui, X. D.; Mu, X. J., Infrared metamaterial for surface-enhanced infrared absorption spectroscopy: pushing the frontier of ultrasensitive on-chip sensing. *Int. J. Optomechatronics* **2021,** 15, 97-119.
89. Li, D. X.; Xu, C.; Xie, J. S.; Lee, C., Research Progress in Surface-Enhanced Infrared Absorption Spectroscopy: From Performance Optimization, Sensing Applications, to System Integration. *Nanomaterials* **2023,** 13.
90. Hartstein, A.; Kirtley, J. R.; Tsang, J. C., Enhancement of the Infrared-Absorption from Molecular Monolayers with Thin Metal Overlayers. *Phys. Rev. Lett.* **1980,** 45, 201-204.
91. Aroca, R. F.; Ross, D. J.; Domingo, C., Surface-enhanced infrared spectroscopy. *Appl. Spectrosc.* **2004,** 58, 324A-338A.
92. Ataka, K.; Heberle, J., Biochemical applications of surface-enhanced infrared absorption spectroscopy. *Anal. Bioanal. Chem.* **2007,** 388, 47-54.
93. Zheludev, N. I., The Road Ahead for Metamaterials. *Science* **2010,** 328, 582-583.
94. Halas, N. J.; Lal, S.; Chang, W. S.; Link, S.; Nordlander, P., Plasmons in Strongly Coupled Metallic Nanostructures. *Chem. Rev.* **2011,** 111, 3913-3961.
95. Brolo, A. G., Plasmonics for future biosensors. *Nat. Photonics* **2012,** 6, 709-713.
96. Yang, X. X.; Sun, Z. P.; Low, T.; Hu, H.; Guo, X. D.; de Abajo, F. J. G.; Avouris, P.; Dai, Q., Nanomaterial-Based Plasmon-Enhanced Infrared Spectroscopy. *Adv. Mater.* **2018,** 30, 1704896.
97. Yang, K.; Yao, X.; Liu, B. W.; Ren, B., Metallic Plasmonic Array Structures: Principles, Fabrications, Properties, and Applications. *Adv. Mater.* **2021**, 2007988.
98. Chen, K.; Adato, R.; Altug, H., Dual-band perfect absorber for multispectral plasmon-enhanced infrared spectroscopy. *ACS Nano* **2012,** 6, 7998-8006.
99. Cerjan, B.; Yang, X.; Nordlander, P.; Halas, N. J., Asymmetric Aluminum Antennas for Self-Calibrating Surface Enhanced Infrared Absorption Spectroscopy. *Acs Photonics* **2016,** 3, 354-360.
100. Cubukcu, E.; Zhang, S.; Park, Y.-S.; Bartal, G.; Zhang, X., Split ring resonator sensors for infrared detection of single molecular monolayers. *Appl. Phys. Lett.* **2009,** 95.
101. Gottheim, S.; Zhang, H.; Govorov, A. O.; Halas, N. J., Fractal nanoparticle plasmonics: the Cayley tree. *ACS Nano* **2015,** 9, 3284-92.
102. Aslan, E.; Aslan, E.; Wang, R.; Hong, M. K.; Erramilli, S.; Turkmen, M.; Saracoglu, O. G.; Dal Negro, L., Multispectral Cesaro-Type Fractal Plasmonic Nanoantennas. *Acs Photonics* **2016,** 3, 2102-2111.
103. Kudyshev, Z. A.; Kildishev, A. V.; Shalaev, V. M.; Boltasseva, A., Machine-learning-assisted metasurface design for high-efficiency thermal emitter optimization. *Applied Physics Reviews* **2020,** 7, 021407.
104. Hwang, I.; Yu, J.; Lee, J.; Choi, J. H.; Choi, D. G.; Jeon, S.; Lee, J.; Jung, J. Y., Plasmon-Enhanced Infrared Spectroscopy Based on Metamaterial Absorbers with Dielectric Nanopedestals. *ACS Photonics* **2018,** 5, 3492-3498.
105. Cetin, A. E.; Etezadi, D.; Altug, H., Accessible Nearfields by Nanoantennas on Nanopedestals for Ultrasensitive Vibrational Spectroscopy. *Adv. Opt. Mater.* **2014,** 2, 866-872.
106. Jung, Y.; Hwang, I.; Yu, J.; Lee, J.; Choi, J. H.; Jeong, J. H.; Jung, J. Y.; Lee, J., Fano Metamaterials on Nanopedestals for Plasmon-Enhanced Infrared Spectroscopy. *Scientific Reports* **2019,** 9.
107. Miao, X.; Yan, L.; Wu, Y.; Liu, P. Q., High-sensitivity nanophotonic sensors with passive trapping of analyte molecules in hot spots. *Light Sci. Appl.* **2021,** 10, 5.

 doi:10.20944/preprints202506.0169.v1

108. Rodrigo, D.; Tittl, A.; Ait-Bouziad, N.; John-Herpin, A.; Limaj, O.; Kelly, C.; Yoo, D.; Wittenberg, N. J.; Oh, S. H.; Lashuel, H. A.; Altug, H., Resolving molecule-specific information in dynamic lipid membrane processes with multi-resonant infrared metasurfaces. *Nat. Commun.* **2018,** 9, 2160.
109. Guo, Q.; Zhu, H.; Liu, F.; Zhu, A. Y.; Reed, J. C.; Yi, F.; Cubukcu, E., Silicon-on-Glass Graphene-Functionalized Leaky Cavity Mode Nanophotonic Biosensor. *Acs Photonics* **2014,** 1, 221-227.
110. John-Herpin, A.; Tittl, A.; Altug, H., Quantifying the Limits of Detection of Surface-Enhanced Infrared Spectroscopy with Grating Order-Coupled Nanogap Antennas. *ACS Photonics* **2018,** 5, 4117-4124.
111. Etezadi, D.; Warner, J. B.; Lashuel, H. A.; Altug, H., Real-Time In Situ Secondary Structure Analysis of Protein Monolayer with Mid-Infrared Plasmonic Nanoantennas. *ACS Sens.* **2018,** 3, 1109-1117.
112. Etezadi, D.; Warner, J. B.; Ruggeri, F. S.; Dietler, G.; Lashuel, H. A.; Altug, H., Nanoplasmonic mid-infrared biosensor for in vitro protein secondary structure detection. *Light Sci. Appl.* **2017,** 6.
113. Hui, X.; Yang, C.; Li, D.; He, X.; Huang, H.; Zhou, H.; Chen, M.; Lee, C.; Mu, X., Infrared Plasmonic Biosensor with Tetrahedral DNA Nanostructure as Carriers for Label-Free and Ultrasensitive Detection of miR-155. *Adv Sci (Weinh)* **2021,** 8, e2100583.
114. John-Herpin, A.; Kavungal, D.; von Mucke, L.; Altug, H., Infrared Metasurface Augmented by Deep Learning for Monitoring Dynamics between All Major Classes of Biomolecules. *Adv. Mater.* **2021**, 2006054.
115. Li, D.; Zhou, H.; Chen, Z.; Ren, Z.; Xu, C.; He, X.; Liu, T.; Chen, X.; Huang, H.; Lee, C.; Mu, X., Ultrasensitive Molecular Fingerprint Retrieval Using Strongly Detuned Overcoupled Plasmonic Nanoantennas. *Adv. Mater.* **2023**, e2301787.
116. Ren, Z.; Zhang, Z.; Wei, J.; Dong, B.; Lee, C., Wavelength-multiplexed hook nanoantennas for machine learning enabled mid-infrared spectroscopy. *Nat. Commun.* **2022,** 13, 3859.
117. Kavungal, D.; Magalhães, P.; Kumar, S. T.; Kolla, R.; Lashuel, H. A.; Altug, H. J. S. A., Artificial intelligence–coupled plasmonic infrared sensor for detection of structural protein biomarkers in neurodegenerative diseases. *Science Advances* **2023,** 9, eadg9644.
118. Zhou, H.; Ren, Z.; Li, D.; Xu, C.; Mu, X.; Lee, C., Dynamic construction of refractive index-dependent vibrations using surface plasmon-phonon polaritons. *Nat. Commun.* **2023,** 14, 7316.
119. Zhou, H.; Li, D.; Ren, Z.; Mu, X.; Lee, C., Loss-induced phase transition in mid-infrared plasmonic metamaterials for ultrasensitive vibrational spectroscopy. *InfoMat* **2022,** 4, e12349.
120. Wei, J.; Li, Y.; Chang, Y.; Hasan, D. M. N.; Dong, B.; Ma, Y.; Qiu, C. W.; Lee, C., Ultrasensitive Transmissive Infrared Spectroscopy via Loss Engineering of Metallic Nanoantennas for Compact Devices. *ACS Appl. Mater. Inter.* **2019,** 11, 47270-47278.
121. Xu, J.; Ren, Z.; Dong, B.; Liu, X.; Wang, C.; Tian, Y.; Lee, C., Nanometer-Scale Heterogeneous Interfacial Sapphire Wafer Bonding for Enabling Plasmonic-Enhanced Nanofluidic Mid-Infrared Spectroscopy. *ACS Nano* **2020,** 14, 12159-12172.
122. Zeng, K.; Wu, C.; Guo, X.; Guan, F.; Duan, Y.; Zhang, L. L.; Yang, X.; Liu, N.; Dai, Q.; Zhang, S., Synthesized complex-frequency excitation for ultrasensitive molecular sensing. *eLight* **2024,** 4.
123. Chang, Y.; Hasan, D.; Dong, B.; Wei, J.; Ma, Y.; Zhou, G.; Ang, K. W.; Lee, C., All-Dielectric Surface-Enhanced Infrared Absorption-Based Gas Sensor Using Guided Resonance. *ACS Appl. Mater. Interfaces* **2018,** 10, 38272-38279.
124. Chong, X. Y.; Zhang, Y. J.; Li, E. W.; Kim, K. J.; Ohodnicki, P. R.; Chang, C. H.; Wang, A. X., Surface-Enhanced Infrared Absorption: Pushing the Frontier for On-Chip Gas Sensing. *Acs Sensors* **2018,** 3, 230-238.
125. Hasan, D.; Lee, C., Hybrid Metamaterial Absorber Platform for Sensing of CO2 Gas at Mid-IR. *Adv. Sci.* **2018,** 5, 1700581.
126. Bareza, N.; Gopalan, K. K.; Alani, R.; Paulillo, B.; Pruneri, V., Mid-infrared Gas Sensing Using Graphene Plasmons Tuned by Reversible Chemical Doping. *Acs Photonics* **2020,** 7, 879-884.
127. Bareza, N., Jr.; Paulillo, B.; Slipchenko, T. M.; Autore, M.; Dolado, I.; Liu, S.; Edgar, J. H.; Vélez, S.; Martín-Moreno, L.; Hillenbrand, R.; Pruneri, V., Phonon-Enhanced Mid-Infrared CO2 Gas Sensing Using Boron Nitride Nanoresonators. *ACS Photonics* **2022,** 9, 34-42.
128. Zhou, H.; Hui, X.; Li, D.; Hu, D.; Chen, X.; He, X.; Gao, L.; Huang, H.; Lee, C.; Mu, X., Metal-Organic Framework-Surface-Enhanced Infrared Absorption Platform Enables Simultaneous On-Chip Sensing of Greenhouse Gases. *Adv. Sci.* **2020,** 7, 2001173.

 doi:10.20944/preprints202506.0169.v1

129. Zhou, H.; Ren, Z.; Xu, C.; Xu, L.; Lee, C., MOF/Polymer-Integrated Multi-Hotspot Mid-Infrared Nanoantennas for Sensitive Detection of CO(2) Gas. *Nano-Micro Lett* **2022,** 14, 207.
130. Hasan, D.; Ho, C. P.; Lee, C., Realization of Fractal-Inspired Thermoresponsive Quasi-3D Plasmonic Metasurfaces with EOT-Like Transmission for Volumetric and Multispectral Detection in the Mid-IR Region. *ACS Omega* **2016,** 1, 818-831.
131. Li, D. X.; Zhou, H.; Hui, X. D.; He, X. M.; Huang, H.; Zhang, J. J.; Mu, X. J.; Lee, C. K.; Yang, Y., Multifunctional Chemical Sensing Platform Based on Dual-Resonant Infrared Plasmonic Perfect Absorber for On-Chip Detection of Poly(ethyl cyanoacrylate). *Adv. Sci.* **2021,** 8, 12.
132. Rodrigo, D.; Tittl, A.; John-Herpin, A.; Limaj, O.; Altug, H., Self-Similar Multiresonant Nanoantenna Arrays for Sensing from Near- to Mid-Infrared. *ACS Photonics* **2018,** 5, 4903-4911.
133. Richter, F. U.; Sinev, I.; Zhou, S.; Leitis, A.; Oh, S. H.; Tseng, M. L.; Kivshar, Y.; Altug, H., Gradient High-Q Dielectric Metasurfaces for Broadband Sensing and Control of Vibrational Light-Matter Coupling. *Adv. Mater.* **2024**, e2314279.
134. Jangid, P.; Richter, F. U.; Tseng, M. L.; Sinev, I.; Kruk, S.; Altug, H.; Kivshar, Y., Spectral Tuning of High-Harmonic Generation with Resonance-Gradient Metasurfaces. *Adv. Mater.* **2023**, e2307494.
135. Liu, S. D.; Leong, E. S.; Li, G. C.; Hou, Y.; Deng, J.; Teng, J. H.; Ong, H. C.; Lei, D. Y., Polarization-Independent Multiple Fano Resonances in Plasmonic Nonamers for Multimode-Matching Enhanced Multiband Second-Harmonic Generation. *ACS Nano* **2016,** 10, 1442-53.
136. Tittl, A.; Leitis, A.; Liu, M.; Yesilkoy, F.; Choi, D. Y.; Neshev, D. N.; Kivshar, Y. S.; Altug, H., Imaging-based molecular barcoding with pixelated dielectric metasurfaces. *Science* **2018,** 360, 1105-1109.
137. Aigner, A.; Tittl, A.; Wang, J.; Weber, T.; Kivshar, Y.; Maier, S. A.; Ren, H., Plasmonic bound states in the continuum to tailor light-matter coupling. *Sci. Adv.* **2022,** 8, eadd4816.
138. Leitis, A.; Tittl, A.; Liu, M.; Lee, B. H.; Gu, M. B.; Kivshar, Y. S.; Altug, H., Angle-multiplexed all-dielectric metasurfaces for broadband molecular fingerprint retrieval. *Sci Adv* **2019,** 5, eaaw2871.
139. Najem, M.; Carcenac, F.; Taliercio, T.; Gonzalez-Posada, F., Aluminum Bowties for Plasmonic-Enhanced Infrared Sensing. *Adv. Opt. Mater.* **2022,** 10.
140. Paggi, L.; Fabas, A.; El Ouazzani, H.; Hugonin, J. P.; Fayard, N.; Bardou, N.; Dupuis, C.; Greffet, J. J.; Bouchon, P., Over-coupled resonator for broadband surface enhanced infrared absorption (SEIRA). *Nat. Commun.* **2023,** 14, 4814.
141. Gu, Y.; You, E. M.; Lin, J. D.; Wang, J. H.; Luo, S. H.; Zhou, R. Y.; Zhang, C. J.; Yao, J. L.; Li, H. Y.; Li, G.; Wang, W. W.; Qiao, Y.; Yan, J. W.; Wu, D. Y.; Liu, G. K.; Zhang, L.; Li, J. F.; Xu, R.; Tian, Z. Q.; Cui, Y.; Mao, B. W., Resolving nanostructure and chemistry of solid-electrolyte interphase on lithium anodes by depth-sensitive plasmon-enhanced Raman spectroscopy. *Nat. Commun.* **2023,** 14, 3536.
142. Leong, S. X.; Leong, Y. X.; Tan, E. X.; Sim, H. Y. F.; Koh, C. S. L.; Lee, Y. H.; Chong, C.; Ng, L. S.; Chen, J. R. T.; Pang, D. W. C.; Nguyen, L. B. T.; Boong, S. K.; Han, X.; Kao, Y.-C.; Chua, Y. H.; Phan-Quang, G. C.; Phang, I. Y.; Lee, H. K.; Abdad, M. Y.; Tan, N. S.; Ling, X. Y., Noninvasive and Point-of-Care Surface-Enhanced Raman Scattering (SERS)-Based Breathalyzer for Mass Screening of Coronavirus Disease 2019 (COVID-19) under 5 min. *ACS Nano* **2022,** 16, 2629-2639.
143. Leong, Y. X.; Lee, Y. H.; Koh, C. S. L.; Phan-Quang, G. C.; Han, X.; Phang, I. Y.; Ling, X. Y., Surface-Enhanced Raman Scattering (SERS) Taster: A Machine-Learning-Driven Multireceptor Platform for Multiplex Profiling of Wine Flavors. *Nano Lett.* **2021,** 21, 2642-2649.
144. Wang, Y.; Zhao, C.; Wang, J.; Luo, X.; Xie, L.; Zhan, S.; Kim, J.; Wang, X.; Liu, X.; Ying, Y., Wearable plasmonic-metasurface sensor for noninvasive and universal molecular fingerprint detection on biointerfaces. *Sci. Adv.* **2021,** 7.
145. Kim, N.; Thomas, M. R.; Bergholt, M. S.; Pence, I. J.; Seong, H.; Charchar, P.; Todorova, N.; Nagelkerke, A.; Belessiotis-Richards, A.; Payne, D. J.; Gelmi, A.; Yarovsky, I.; Stevens, M. M., Surface enhanced Raman scattering artificial nose for high dimensionality fingerprinting. *Nat. Commun.* **2020,** 11, 207.
146. Son, W. K.; Choi, Y. S.; Han, Y. W.; Shin, D. W.; Min, K.; Shin, J.; Lee, M. J.; Son, H.; Jeong, D. H.; Kwak, S. Y., In vivo surface-enhanced Raman scattering nanosensor for the real-time monitoring of multiple stress signalling molecules in plants. *Nat. Nanotechnol.* **2023,** 18, 205-216.

 doi:10.20944/preprints202506.0169.v1

147. Zhao, Y.; Askarpour, A. N.; Sun, L.; Shi, J.; Li, X.; Alu, A., Chirality detection of enantiomers using twisted optical metamaterials. *Nat. Commun.* **2017,** 8, 14180.
148. Hendry, E.; Carpy, T.; Johnston, J.; Popland, M.; Mikhaylovskiy, R. V.; Lapthorn, A. J.; Kelly, S. M.; Barron, L. D.; Gadegaard, N.; Kadodwala, M., Ultrasensitive detection and characterization of biomolecules using superchiral fields. *Nat. Nanotechnol.* **2010,** 5, 783-787.
149. Kakkar, T.; Keijzer, C.; Rodier, M.; Bukharova, T.; Taliansky, M.; Love, A. J.; Milner, J. J.; Karimullah, A. S.; Barron, L. D.; Gadegaard, N.; Lapthorn, A. J.; Kadodwala, M., Superchiral near fields detect virus structure. *Light Sci. Appl.* **2020,** 9.
150. Hajji, M.; Cariello, M.; Gilroy, C.; Kartau, M.; Syme, C. D.; Karimullah, A.; Gadegaard, N.; Malfait, A.; Woisel, P.; Cooke, G.; Peveler, W. J.; Kadodwala, M., Chiral Quantum Metamaterial for Hypersensitive Biomolecule Detection. *ACS Nano* **2021,** 15, 19905-19916.
151. Tabouillot, V.; Kumar, R.; Lalaguna, P. L.; Hajji, M.; Clarke, R.; Karimullah, A. S.; Thomson, A. R.; Sutherland, A.; Gadegaard, N.; Hashiyada, S.; Kadodwala, M., Near-Field Probing of Optical Superchirality with Plasmonic Polarized Luminescence for Enhanced Bio-Detection. *Acs Photonics* **2022,** 9, 3617-3624.
152. Mohammadi, E.; Tavakoli, A.; Dehkhoda, P.; Jahani, Y.; Tsakmakidis, K. L.; Tittl, A.; Altug, H., Accessible Superchiral Near-Fields Driven by Tailored Electric and Magnetic Resonances in All-Dielectric Nanostructures. *ACS Photonics* **2019,** 6, 1939-1946.
153. Kim, R. M.; Huh, J. H.; Yoo, S.; Kim, T. G.; Kim, C.; Kim, H.; Han, J. H.; Cho, N. H.; Lim, Y. C.; Im, S. W.; Im, E.; Jeong, J. R.; Lee, M. H.; Yoon, T. Y.; Lee, H. Y.; Park, Q. H.; Lee, S.; Nam, K. T., Enantioselective sensing by collective circular dichroism. *Nature* **2022,** 612, 470-476.
154. Keiderling, T. A., Protein and peptide secondary structure and conformational determination with vibrational circular dichroism. *Curr. Opin. Chem. Biol.* **2002,** 6, 682-688.
155. Vázquez-Guardado, A.; Chanda, D., Superchiral Light Generation on Degenerate Achiral Surfaces. *Phys. Rev. Lett.* **2018,** 120.
156. Xu, C.; Ren, Z.; Zhou, H.; Zhou, J.; Li, D.; Lee, C., Near-Field Coupling Induced Less Chiral Responses in Chiral Metamaterials for Surface-Enhanced Vibrational Circular Dichroism. *Adv. Funct. Mater.* **2023**, 2314482.
157. Xu, C.; Ren, Z.; Zhou, H.; Zhou, J.; Ho, C. P.; Wang, N.; Lee, C., Expanding chiral metamaterials for retrieving fingerprints via vibrational circular dichroism. *Light Sci. Appl.* **2023,** 12, 154.
158. Kurouski, D., Advances of Vibrational Circular Dichroism (VCD) in bioanalytical chemistry. A review. *Anal. Chim. Acta* **2017,** 990, 54-66.
159. Janesko, B. G.; Scuseria, G. E., Surface enhanced Raman optical activity of molecules on orientationally averaged substrates: Theory of electromagnetic effects. *J. Chem. Phys.* **2006,** 125.
160. Sun, M. T.; Zhang, Z. L.; Wang, P. J.; Li, Q.; Ma, F. C.; Xu, H. X., Remotely excited Raman optical activity using chiral plasmon propagation in Ag nanowires. *Light Sci. Appl.* **2013,** 2.
161. Pour, S. O.; Rocks, L.; Faulds, K.; Graham, D.; Parchansky, V.; Bour, P.; Blanch, E. W., Through-space transfer of chiral information mediated by a plasmonic nanomaterial. *Nat. Chem.* **2015,** 7, 591-596.
162. Ma, W.; Cheng, F.; Liu, Y., Deep-Learning-Enabled On-Demand Design of Chiral Metamaterials. *ACS Nano* **2018,** 12, 6326-6334.
163. Choi, W. J.; Cheng, G.; Huang, Z. Y.; Zhang, S.; Norris, T. B.; Kotov, N. A., Terahertz circular dichroism spectroscopy of biomaterials enabled by kirigami polarization modulators. *Nat. Mater.* **2019,** 18, 820-826.
164. McDonnell, C.; Deng, J. H.; Sideris, S.; Ellenbogen, T.; Li, G. X., Functional THz emitters based on Pancharatnam-Berry phase nonlinear metasurfaces. *Nat. Commun.* **2021,** 12.
165. Choi, W. J.; Yano, K.; Cha, M.; Colombari, F. M.; Kim, J. Y.; Wang, Y. C.; Lee, S. H.; Sun, K.; Kruger, J. M.; De Moura, A. F.; Kotov, N. A., Chiral phonons in microcrystals and nanofibrils of biomolecules. *Nat. Photonics* **2022,** 16, 366-+.
166. Kim, M.; Tsukruk, V. V., Spectroscopy finds chiral phonons. *Nat. Photonics* **2022,** 16, 337-338.
167. Probst, P. T.; Mayer, M.; Gupta, V.; Steiner, A. M.; Zhou, Z.; Auernhammer, G. K.; König, T. A. F.; Fery, A., Mechano-tunable chiral metasurfaces via colloidal assembly. *Nat. Mater.* **2021,** 20, 1024-1028.
168. Drexhage, K.; Kuhn, H.; Schäfer, F., Variation of the fluorescence decay time of a molecule in front of a mirror. *Berichte der Bunsengesellschaft für physikalische Chemie* **1968,** 72, 329-329.

 doi:10.20944/preprints202506.0169.v1

169. Lakowicz, J. R., Radiative decay engineering: Biophysical and biomedical applications. *Anal. Biochem.* **2001,** 298, 1-24.
170. Geddes, C. D.; Gryczynski, I.; Malicka, J.; Gryczynski, Z.; Lakowicz, J. R., Metal-enhanced fluorescence: Potential applications in HTS. *Comb. Chem. High Throughput Screening* **2003,** 6, 109-117.
171. Aslan, K.; Lakowicz, J. R.; Szmacinski, H.; Geddes, C. D., Metal-enhanced fluorescence solution-based sensing platform. *J. Fluoresc.* **2004,** 14, 677-679.
172. Aslan, K.; Gryczynski, I.; Malicka, J.; Matveeva, E.; Lakowicz, J. R.; Geddes, C. D., Metal-enhanced fluorescence: an emerging tool in biotechnology. *Curr. Opin. Biotechnol.* **2005,** 16, 55-62.
173. Lakowicz, J. R.; Geddes, C. D.; Gryczynski, I.; Malicka, J.; Gryczynski, Z.; Aslan, K.; Lukomska, J.; Matveeva, E.; Zhang, J. A.; Badugu, R.; Huang, J., Advances in surface-enhanced fluorescence. *J. Fluoresc.* **2004,** 14, 425-441.
174. Aslan, K.; Lakowicz, J. R.; Geddes, C. D., Metal-enhanced fluorescence using anisotropic silver nanostructures: critical progress to date. *Anal. Bioanal. Chem.* **2005,** 382, 926-933.
175. Schalkhammer, T.; Aussenegg, F. R.; Leitner, A.; Brunner, H.; Hawa, G.; Lobmaier, C.; Pittner, F. In *Detection of fluorophore-labelled antibodies by surface-enhanced fluorescence on metal nanoislands*, Conference on Biomedical Sensing, Imaging, and Tracking Technologies II, San Jose, Ca, Feb 11-13, 1997; San Jose, Ca, 1997; pp 129-136.
176. Lakowicz, J. R.; Shen, B.; Gryczynski, Z.; D'Auria, S.; Gryczynski, I., Intrinsic fluorescence from DNA can be enhanced by metallic particles. *Biochem. Biophys. Res. Commun.* **2001,** 286, 875-879.
177. Matveeva, E. G.; Gryczynski, Z.; Lakowicz, J. R., Myoglobin immunoassay based on metal particle-enhanced fluorescence. *J. Immunol. Methods* **2005,** 302, 26-35.
178. Liz-Marzán, L. M., Tailoring surface plasmons through the morphology and assembly of metal nanoparticles. *Langmuir* **2006,** 22, 32-41.
179. Xia, Y. N.; Xiong, Y. J.; Lim, B.; Skrabalak, S. E., Shape-Controlled Synthesis of Metal Nanocrystals: Simple Chemistry Meets Complex Physics? *Angewandte Chemie-International Edition* **2009,** 48, 60-103.
180. Tang, F.; He, F.; Cheng, H. C.; Li, L. D., Self-Assembly of Conjugated Polymer-Ag@SiO₂ Hybrid Fluorescent Nanoparticles for Application to Cellular Imaging. *Langmuir* **2010,** 26, 11774-11778.
181. Li, H.; Qiang, W. B.; Vuki, M.; Xu, D. K.; Chen, H. Y., Fluorescence Enhancement of Silver Nanoparticle Hybrid Probes and Ultrasensitive Detection of IgE. *Anal. Chem.* **2011,** 83, 8945-8952.
182. Kühn, S.; Håkanson, U.; Rogobete, L.; Sandoghdar, V., Enhancement of single-molecule fluorescence using a gold nanoparticle as an optical nanoantenna. *Phys. Rev. Lett.* **2006,** 97.
183. Taminiau, T. H.; Stefani, F. D.; Segerink, F. B.; Van Hulst, N. F., Optical antennas direct single-molecule emission. *Nat. Photonics* **2008,** 2, 234-237.
184. Kinkhabwala, A.; Yu, Z. F.; Fan, S. H.; Avlasevich, Y.; Müllen, K.; Moerner, W. E., Large single-molecule fluorescence enhancements produced by a bowtie nanoantenna. *Nat. Photonics* **2009,** 3, 654-657.
185. Fromm, D. P.; Sundaramurthy, A.; Schuck, P. J.; Kino, G.; Moerner, W. E., Gap-dependent optical coupling of single "Bowtie" nanoantennas resonant in the visible. *Nano Lett.* **2004,** 4, 957-961.
186. Punj, D.; Mivelle, M.; Moparthi, S. B.; van Zanten, T. S.; Rigneault, H.; van Hulst, N. F.; García-Parajó, M. F.; Wenger, J., A plasmonic 'antenna-in-box' platform for enhanced single-molecule analysis at micromolar concentrations. *Nat. Nanotechnol.* **2013,** 8, 512-516.
187. Bardhan, R.; Grady, N. K.; Cole, J. R.; Joshi, A.; Halas, N. J., Fluorescence Enhancement by Au Nanostructures: Nanoshells and Nanorods. *ACS Nano* **2009,** 3, 744-752.
188. Khatua, S.; Paulo, P. M. R.; Yuan, H. F.; Gupta, A.; Zijlstra, P.; Orrit, M., Resonant Plasmonic Enhancement of Single-Molecule Fluorescence by Individual Gold Nanorods. *ACS Nano* **2014,** 8, 4440-4449.
189. Ray, K.; Badugu, R.; Lakowicz, J. R., Sulforhodamine adsorbed Langmuir-Blodgett layers on silver island films: Effect of probe distance on the metal-enhanced fluorescence. *J. Phys. Chem. C* **2007,** 111, 7091-7097.
190. Luan, J.; Seth, A.; Gupta, R.; Wang, Z.; Rathi, P.; Cao, S.; Gholami Derami, H.; Tang, R.; Xu, B.; Achilefu, S.; Morrissey, J. J.; Singamaneni, S., Ultrabright fluorescent nanoscale labels for the femtomolar detection of analytes with standard bioassays. *Nat. Biomed. Eng.* **2020,** 4, 518-530.

 doi:10.20944/preprints202506.0169.v1

191. Lin, Z.; Liu, M.; Xing, W.; Wang, F.; Zhang, H.; Wei, X.; Schmitthenner, H.; Xie, X.; Xia, X.; Yang, J., A near-infrared fluorescence-enhancing plasmonic biosensing microarray identifies soluble PD-L1 and ICAM-1 as predictive checkpoint biomarkers for cancer immunotherapy. *Biosens. Bioelectron.* **2023,** 240, 115633.
192. Chowdhury, M. H.; Ray, K.; Gray, S. K.; Pond, J.; Lakowicz, J. R., Aluminum Nanoparticles as Substrates for Metal-Enhanced Fluorescence in the Ultraviolet for the Label-Free Detection of Biomolecules. *Anal. Chem.* **2009,** 81, 1397-1403.
193. Chen, Z.; Li, H.; Jia, W. C.; Liu, X. H.; Li, Z. M.; Wen, F.; Zheng, N.; Jiang, J. D.; Xu, D. K., Bivalent Aptasensor Based on Silver-Enhanced Fluorescence Polarization for Rapid Detection of Lactoferrin in Milk. *Anal. Chem.* **2017,** 89, 5901-5909.
194. Li, C. Y.; Duan, S.; Yi, J.; Wang, C.; Radjenovic, P. M.; Tian, Z. Q.; Li, J. F., Real-time detection of single-molecule reaction by plasmon-enhanced spectroscopy. *Science Advances* **2020,** 6.
195. Acuna, G. P.; Möller, F. M.; Holzmeister, P.; Beater, S.; Lalkens, B.; Tinnefeld, P., Fluorescence Enhancement at Docking Sites of DNA-Directed Self-Assembled Nanoantennas. *Science* **2012,** 338, 506-510.
196. Lu, H. P.; Xie, X. S., Single-molecule spectral fluctuations at room temperature. *Nature* **1997,** 385, 143-146.
197. Tenopala-Carmona, F.; Fronk, S.; Bazan, G. C.; Samuel, I. D. W.; Penedo, J. C., Real-time observation of conformational switching in single conjugated polymer chains. *Science Advances* **2018,** 4.
198. Abdulhalim, I.; Karabchevsky, A.; Patzig, C.; Rauschenbach, B.; Fuhrmann, B.; Eltzov, E.; Marks, R.; Xu, J.; Zhang, F.; Lakhtakia, A., Surface-enhanced fluorescence from metal sculptured thin films with application to biosensing in water. *Appl. Phys. Lett.* **2009,** 94.
199. Hu, R. B.; Yang, Y.; Liu, Y.; Liao, T.; Liu, Y. Y.; Tang, J. H.; Wang, G. H.; Wang, G. X.; Liang, Y. Y.; Yuan, J.; Zhang, B., Multiplexed evaluation of immunity against SARS-CoV-2 variants using surface enhanced fluorescence from a nanostructured plasmonic chip. *J. Nanobiotechnol.* **2022,** 20.
200. Zhu, J. L.; Zhao, X.; Ouyang, J.; Na, N.; Mao, J. P., Single-Molecule Evaluation of the SARS-CoV-2 Nucleocapsid Protein Using Gold Particle-in-a-Frame Nanostructures Enhanced Fluorescent Assay. *Anal. Chem.* **2023,** 95, 5267-5274.
201. Yan, Y.; Zhang, C.; Zheng, J. Y.; Yao, J.; Zhao, Y. S., Optical modulation based on direct photon-plasmon coupling in organic/metal nanowire heterojunctions. *Adv. Mater.* **2012,** 24, 5681-6.
202. Liu, X.; Zhang, Q.; Yip, J. N.; Xiong, Q.; Sum, T. C., Wavelength tunable single nanowire lasers based on surface plasmon polariton enhanced Burstein-Moss effect. *Nano Lett.* **2013,** 13, 5336-43.
203. Xu, Q.; Schmidt, B.; Pradhan, S.; Lipson, M., Micrometre-scale silicon electro-optic modulator. *Nature* **2005,** 435, 325-7.
204. Melikyan, A.; Alloatti, L.; Muslija, A.; Hillerkuss, D.; Schindler, P. C.; Li, J.; Palmer, R.; Korn, D.; Muehlbrandt, S.; Van Thourhout, D.; Chen, B.; Dinu, R.; Sommer, M.; Koos, C.; Kohl, M.; Freude, W.; Leuthold, J., High-speed plasmonic phase modulators. *Nat. Photonics* **2014,** 8, 229-233.
205. Neutens, P.; Van Dorpe, P.; De Vlaminck, I.; Lagae, L.; Borghs, G., Electrical detection of confined gap plasmons in metal–insulator–metal waveguides. *Nat. Photonics* **2009,** 3, 283-286.
206. Ming, T.; Zhao, L.; Xiao, M.; Wang, J., Resonance-coupling-based plasmonic switches. *Small* **2010,** 6, 2514-9.
207. Sorger, V. J.; Oulton, R. F.; Ma, R.-M.; Zhang, X., Toward integrated plasmonic circuits. *MRS Bull.* **2012,** 37, 728-738.
208. Liu, X.; Zhang, Z.; Zhou, J.; Liu, W.; Zhou, G.; Lee, C., Development of Photonic In-Sensor Computing Based on a Mid-Infrared Silicon Waveguide Platform. *ACS Nano* **2024,** 18, 22938-22948.
209. Liu, X.; Zhang, Z.; Zhou, J.; Liu, W.; Zhou, G.; Lee, C., Artificial Intelligence-Enhanced Waveguide "Photonic Nose"- Augmented Sensing Platform for VOC Gases in Mid-Infrared. *Small* **2024**, e2400035.
210. Ren, Z.; Zhang, Z.; Zhuge, Y.; Xiao, Z.; Xu, S.; Zhou, J.; Lee, C., Near-Sensor Edge Computing System Enabled by a CMOS Compatible Photonic Integrated Circuit Platform Using Bilayer AlN/Si Waveguides. *Nanomicro Lett* **2025,** 17, 261.

 doi:10.20944/preprints202506.0169.v1

disclaim responsibility for any injury to people or property resulting from any ideas, methods, instructions or products referred to in the content.